NASA TECHNICAL NOTE

NASA TN D-2929

LOAN COPY: RE
AFWL (W
KIRTLAND AF

TECH LIBRARY KAFB, NM
0154770

NASA TN D-2929

# BASE PRESSURES AND CONVECTIVE HEAT-TRANSFER COEFFICIENTS FOR CLUSTERED SONIC NOZZLES WITH EMPHASIS ON CHOKED EXHAUST BACKFLOW

*by John P. Weidner and James M. Cubbage*

*Langley Research Center*
*Langley Station, Hampton, Va.*

NATIONAL AERONAUTICS AND SPACE ADMINISTRATION • WASHINGTON, D. C. • SEPTEMBER 1965

TECH LIBRARY KAFB, NM
0154770

# BASE PRESSURES AND CONVECTIVE HEAT-TRANSFER COEFFICIENTS FOR CLUSTERED SONIC NOZZLES WITH EMPHASIS ON CHOKED EXHAUST BACKFLOW

By John P. Weidner and James M. Cubbage

Langley Research Center
Langley Station, Hampton, Va.

NATIONAL AERONAUTICS AND SPACE ADMINISTRATION

For sale by the Clearinghouse for Federal Scientific and Technical Information
Springfield, Virginia 22151 – Price $2.00

# BASE PRESSURES AND CONVECTIVE HEAT-TRANSFER COEFFICIENTS FOR CLUSTERED SONIC NOZZLES WITH EMPHASIS ON CHOKED EXHAUST BACKFLOW

By John P. Weidner and James M. Cubbage
Langley Research Center

## SUMMARY

A base heating investigation has been conducted to determine local heat-transfer coefficients and pressures due to backflowing exhaust gases from clusters of three and four sonic nozzles. This investigation was concerned with the condition for which backflowing exhaust gases become confined within the nozzle cluster and choke at the minimum area between adjacent nozzles. The models simulated nozzle arrangements of typical launch vehicles, and data were obtained over a range of nozzle spacings, nozzle extensions beyond the base plate, and nozzle total pressures.

It was found that the highest pressures and heat-transfer coefficients generally occurred at the base center, with a second but smaller rise in heat-transfer coefficient occurring between adjacent nozzles. Base pressure and heat-transfer coefficients were reduced by increasing either the nozzle spacing or the nozzle extension, and the highest values were observed for the four-nozzle models. A direct proportionality was found between the pressures and heat-transfer coefficients at the base center. At a common base-center pressure, less heat transfer occurs for the larger nozzle spacings and for the smaller nozzle extensions.

## INTRODUCTION

High-altitude operation of launch vehicles containing clustered propulsive nozzles leads to interaction between adjacent exhaust plumes and consequent backflow of hot exhaust gases into the base region. The only escape route for the exhaust backflow, trapped within the nozzle cluster, is through the area between adjacent nozzles (window area). At sufficiently high altitudes the backflow becomes great enough to choke the cluster aerodynamically, making it impossible for cooler ambient air to enter or influence the base region. This flow phenomenon yields pressures within the base region that are much higher than the ambient pressure and introduces extremely high heating rates, making an adequate thermal design necessary for the protection of the base and component parts contained within the nozzle cluster.

The problem of protecting the base region from excessive heating caused by backflow from clustered propulsive nozzles has been recognized for the past several years. The research to date has been primarily concerned with heat-flux and pressure measurements on the base of various clustered-rocket configurations, along with some studies of the backflow characteristics involved. (See, for example, refs. 1 to 4.) Also, heat-transfer and pressure data have been reported on models of specific launch-vehicle designs, such as Saturn. (See refs. 5 and 6.) However, these tests were usually conducted with external flow either under conditions for which choking of the backflow within the cluster did not exist or for which base pressures were of predominant interest. The present investigation was designed to provide base-pressure and heat-transfer-coefficient data for clusters of three and four sonic nozzles over a range of nozzle spacings and nozzle pressures for the high-heating condition of choked backflow within the nozzle cluster.

The investigation reported herein was conducted in a blowdown facility employing air at ambient temperature exhausting to atmospheric pressure. The spacings between nozzles were 0.35, 0.50, and 0.75 nozzle diameter; nozzle extensions from the base were 0, 0.5, 1.0, and 1.5 nozzle diameters; and nozzle total pressure ranged from 350 to 550 psia.

## SYMBOLS

| | |
|---|---|
| $A$ | area, square inches |
| $A_n$ | area bounded by nozzles in plane of nozzle exits, square inches (see fig. 2) |
| $A_s$ | sum of minimum areas between nozzles, bounded by nozzle-exit plane and base plate, square inches (see fig. 2) |
| $A_t$ | sum of triangular areas between nozzles, bounded by nozzle-exit plane and exhaust plumes, square inches (see fig. 4) |
| $A_w$ | total window area between nozzles, $A_s + A_t$, square inches |
| $a$ | sonic velocity, feet per second |
| $C_t$ | distance in plane of nozzle exits between inside diameters of adjacent nozzles, inches |
| $c$ | specific heat, Btu/lb-$^\circ$R |
| $d$ | diameter, inches |
| $h$ | heat-transfer coefficient measured on base, Btu/ft$^2$-sec-$^\circ$R |
| $k$ | thermal conductivity, Btu/ft$^2$-sec-$^\circ$R/ft |

| | |
|---|---|
| $N$ | number of nozzles |
| $N_{St}$ | Stanton number |
| $p$ | pressure, pounds per square inch absolute |
| $p_t$ | total pressure as measured in the settling chamber, pounds per square inch absolute |
| $q$ | heat flux per unit area, $Btu/ft^2\text{-}sec$ |
| $R$ | Reynolds number |
| $r$ | radial distance from center of base, inches |
| $r_o$ | radial distance from center of base to point of minimum distance between adjacent nozzles, inches (see fig. 2) |
| $s$ | distance from base plate to nozzle-exit plane, inches |
| $T$ | temperature, degrees F |
| $\Delta T$ | incremental temperature |
| $T_g$ | total temperature of exhaust gases on base, degrees F |
| $T_t$ | total temperature as measured in settling chamber, degrees F |
| $t$ | time, seconds |
| $\Delta t$ | incremental time, seconds |
| $V$ | velocity, feet per second |
| $\mu$ | viscosity, $lb\text{-}sec/ft^2$ |
| $\rho$ | density, $lb\text{-}sec^2/ft^4$ |

Subscripts:

| | |
|---|---|
| a | ambient conditions |
| c | conditions at base center |
| e | conditions at nozzle exit |
| w | conditions at base window |

## APPARATUS AND METHOD

### Test Apparatus and Models

This experimental investigation was conducted in a blowdown facility with the test apparatus as shown schematically in figure 1. The basic apparatus consisted of a cylindrical settling chamber, a secondary base plate that contained the sonic nozzles, and a base plate which contained the pressure and temperature instrumentation. In addition to a balsa insulating plate used to reduce heat conduction to other parts of the test apparatus, several spacing plates were used to provide the desired nozzle extension. Air was supplied to the settling chamber from an air supply system consisting of three storage tanks, each with a 1000-cubic-foot capacity, and was exhausted from the sonic nozzles to atmospheric pressure.

Spacer plates were constructed from micarta and were of a thickness such that the desired nozzle extension could be obtained by their addition or removal; a different set of plates was required for each nozzle spacing tested for both the three- and four-nozzle configurations. The instrumented base, fabricated from a sheet of 1/32-inch inconel, was made as thin as practical in order to have a small thermal capacity so that heat flux could be determined more accurately from measurements of time rates of change of base temperatures. The holes in the base plate through which the sonic nozzles extended were made 1/32 inch larger than the outside diameter of the sonic nozzles to prevent contact of the nozzles with the base plate, thereby eliminating heat losses by conduction.

The sonic nozzles, which were 2.750 inches long, were made of stainless steel with an outside diameter of 0.875 inch and an inside diameter of 0.750 inch. A sketch of the three- and four-nozzle configurations and a list of the various geometric parameters used are presented in figure 2. Each geometric configuration was tested at nozzle total pressures ranging from about 350 to 550 psia and at a supply temperature of about 80° F.

### Instrumentation

The total pressure and temperature of the air supply in the settling chamber were measured by the instrumentation shown in figure 1. The base instrumentation consisted of static-pressure orifices and thermocouples mounted in the base plate. Two sets of tests were required in order to obtain both a pressure and temperature measurement at the center of the base plate. Location of the base instrumentation for the first set of tests is illustrated in the sketch of table I. The pressure-orifice and thermocouple locations are given as a ratio of the radial location of the instrumentation to the radius at the point of minimum distance between adjacent nozzles $r/r_o$. In all cases, a pressure orifice and thermocouple were located on the line of minimum distance between adjacent nozzles.

Models for the second set of tests contained instrumentation located as shown in the sketch of table II. These models contained a limited number of static-pressure orifices, located the same as for the first set of tests, in order to insure that the flow conditions were similar in both cases. Plate-center pressures at a common nozzle total pressure were assumed to be the same for both sets of tests. Thermocouple locations were confined to an area within the nozzle cluster in order to obtain a more complete survey in the area of particular interest. In these models a thermocouple was located at the base center in order to measure a stagnation-point heat-transfer coefficient of the backflowing gases. Additional tests were conducted in order to obtain schlieren photographs of the backflow phenomenon and the flow characteristics at the base plate.

The static-pressure orifices, with inside diameters of 0.020 inch, were connected to pressure transducers which were in turn connected to a continuously recording oscillograph. Temperature instrumentation consisted of No. 30 iron and constantan thermocouples spot-welded to the underside of the base plate. All thermocouple wires were connected to a recording oscillograph.

## Procedure

For each nozzle-cluster configuration, data were taken at five nozzle total pressures at intervals of about 50 psi between 350 and 550 psia. Before each test the base plate was chilled with dry ice to about $-100^{\circ}$ F to provide an initial temperature difference between the plate and the exhaust gas and hence provide a sufficiently high heat flux into the plate to increase the accuracy of the measurements. As soon as the base was chilled, air at the desired total pressure was admitted to the settling chamber and pressure and temperature data were recorded. Although the pressure and temperature data of greatest interest were recorded during the first few seconds of each test, these data were recorded continuously over the time period required for the supply pressure to decrease 50 psi. At this point, the air supply was cut off and the base was rechilled for a new test. Thus, continuous pressure data were obtained over the supply-pressure range from 350 to 550 psia. Chilling of the model caused some frosting of the base plate, but this frost was observed to disappear immediately after the air was admitted to the settling chamber. Consequently, the frost was not considered to be a factor in determining heat-transfer coefficients.

## Analysis of Heat-Transfer Data

The temperature data obtained in these tests were converted into a heat-transfer coefficient which is defined as the heat flux into the plate divided by a temperature difference. Since the base plate was thin and had a low thermal conductivity, lateral conduction was assumed negligible so that a unit area of the base plate was essentially a calorimeter. The heat flux per unit area was thus calculated from the product of the time rate of change of plate temperature and the thermal capacity of the plate. Radiation was considered

negligible since the exhausting air was at a low temperature. The properties of the inconel base plate and the heat-flux equation are:

| | |
|---|---|
| Specific heat, c, Btu/lb-$^{o}$R | 0.095 |
| Specific volume, v, ft$^{3}$/lb | 0.00188 |
| Conductivity, k, Btu/ft$^{2}$-hr-$^{o}$R/ft | 8.5 |
| Plate thickness, x, ft | 0.00260 |
| Thermal capacity, $\frac{cx}{v}$, Btu/ft$^{2}$-$^{o}$R | 0.131 |

$$q = \frac{cx}{v}\frac{\Delta T}{\Delta t}$$

The temperature difference used to calculate the heat-transfer coefficient is normally based on the difference between the adiabatic wall temperature and the plate temperature, but with the limited pressure data of this investigation it was not possible to establish with accuracy the true adiabatic wall temperature along the plate. However, this adiabatic wall temperature would not ordinarily be a known parameter to a designer making use of these heat-transfer coefficients. Hence, the heat-transfer coefficient has been defined on the basis of the difference between the total temperature of the exhaust gases and the plate temperature. Although the plate was thin, the temperature drop through the plate resulted in a low measured plate temperature and required a correction to the data. The temperature drop was calculated on the assumption that the heat flux into the plate was constant at any specific time. It was found that $\Delta T = 0.55q$, which amounts to about 10% of the total temperature difference. This result may be obtained from the temperature response chart on page 119 in reference 7. With this correction, the equation to determine heat-transfer coefficient is:

$$h = \frac{q}{T_t - (T + 0.55q)}$$

Typical temperature responses for thermocouples at the center of the base cluster, at the window, and in the settling chamber are shown in the upper left-hand corner of figure 3. The rise of the total temperature is due to a compression of the air contained in the piping and the settling chamber when the valve upstream of the settling chamber is opened. The lag in response of the base temperature represents the time required for the air supply valve to open and the desired total pressure to become established in the settling chamber (upper right-hand corner of fig. 3).

After 10 seconds the temperatures in the settling chamber and at the base-plate center and window positions leveled off to about 87$^{o}$ F, 84$^{o}$ F, and 70$^{o}$ F, respectively, approaching equilibrium conditions. The small difference between $T_t$ and $T_c$ is thought to represent a small amount of lateral conduction due to the colder portion of the base outside the cluster. The difference between $T_c$ and $T_w$ represents the difference between the total temperature and the

adiabatic wall temperature which would occur in a laminar flow at a Mach number of 1.0.

Heat-flux and heat-transfer-coefficient data calculated from the temperature data at 0.1-second intervals are presented in the lower portion of figure 3, with the temperature drop through the plate taken into account in the heat-transfer coefficients. Theoretically, the heat-transfer coefficient should have remained constant once the backflow was established in the model; however, because of small heat losses present in the test setup, the heat-transfer coefficient decreases with time. The primary cause of this decrease is thought to be lateral conduction along the plate. The increasing temperature difference between $T_c$ and $T_w$ with increasing time is indicative of an increase in lateral heat conduction. There is also a simultaneous decrease of heat flux into the plate. A combination of these two factors accounts for the increasing influence of lateral conduction and consequent decrease in heat-transfer coefficient. The dashed portion of the heat-flux curve represents the heat flux required to produce a constant heat-transfer coefficient. Errors in heat-flux measurements due to conduction losses from the back of the base plate were minimized by a groove, 1/4 inch wide and 3/16 inch deep, cut into the balsa insulating plate directly under the thermocouple locations. Since the temperatures on the base showed no significant change until after 0.4 second, the testing time before the desired heat-transfer coefficients were obtained was about 0.5 second. Because of the difference between the adiabatic wall temperature at the window and the total temperature, which is approximately the same as the difference between $T_c$ and $T_w$ after 10 seconds, the heat-transfer coefficients calculated in the region of the window are about 10% lower than the heat-transfer coefficient based on recovery temperature.

Because of the rise and fall of heat-transfer coefficient with time caused by the pressure rise in the settling chamber and subsequent lateral conduction along the plate, it was necessary to calculate values of heat-transfer coefficient at 0.1-second intervals until the peak value was found. This maximum value was then considered to be the desired heat-transfer coefficient for the given operating conditions. It is believed that heat-transfer coefficients calculated as outlined are within the accuracy of the error involved, generally less than 10%. The error comes about through taking the slopes of the temperature-time curves.

## FLOW MODEL

The exhaust-gas backflow and resulting base pressures associated with the three- and four-nozzle clusters are a result of a complicated flow pattern set up by the impinging exhaust plumes. In order that the experimental results might be better understood, a flow model was constructed to determine some of the mechanics behind the base-backflow phenomenon.

A sketch of typical three- and four-nozzle clusters is shown in figure 4; points between adjacent nozzles, where jet-boundary streamlines from the neighboring plumes impinge, describe a line which is designated the "line of

impingement." Along this line, oblique or normal shocks formed by plumes impinging on each other produce high-pressure regions and subsequent mass removal or exhaust backflow from the streamlines. Details of the origin of the exhaust backflow from intersecting streamlines are given in references 1 and 2. For a given nozzle configuration, major factors which influence the amount of backflow are the pressure rise across the shock wave along the line of impingement and the mixing length along individual impinging streamlines measured from the nozzle exit to the point of impingement. At the minimum distance between adjacent nozzles there is a maximum angle of impingement and a minimum mixing length. By following along the line of impingement away from this point, it can be seen that the angle between impinging streamlines and the subsequent shock wave decreases while the mixing length increases. When the local backflow is assumed to be directly proportional to the mixing length, simplified calculations indicate that the mixing length has the greatest influence on exhaust backflow; hence, greater backflow might be expected a short distance away from the point of minimum distance between the nozzles.

Lines of impingement, originating from neighboring nozzles forming the cluster, converge over the center of the base; this convergence causes a large amount of exhaust backflow from this point. The subsequent stream of high-energy backflow from this common point of intersection produces a high pressure at the center of the base which is greater than that produced from the backflow originating at other points along the line of impingement. A total-pressure gradient should therefore exist across the base in which the average total pressure at the window is less than that measured at the base center. This assumed flow model is supported by total-pressure data along the base of a four-nozzle cluster presented in reference 2 in which the greater total pressure is shown to occur at the base center. The magnitude of this high local pressure at the base center is highly dependent on the amount of nozzle extension from the base, since a large nozzle extension would allow more room for the core of high-energy backflow to mix with adjacent low-energy backflow. Or, if supersonic backflow is developed in the high-energy core of backflowing gas through mass addition, as discussed in reference 2, the greater nozzle extension will allow more room for further expansion and subsequent greater total-pressure losses through the normal shock "standing off" the base. Also presented in reference 2 are total-pressure distributions, measured perpendicular to the base plate at the window location, which show the higher total pressures at the base, with the total pressure decreasing with increased distance above the base. The cause of this change in total pressure was attributed to streamlines near the base at the window originating from backflow near the base center, whereas streamlines at greater distances above the base originate from low-energy backflow near the window. This total-pressure gradient at the window may result in mixed flow when it is assumed that there is no static-pressure gradient; that is, the backflow would be sonic near the base but would be subsonic at the top portions of the window.

## RESULTS AND DISCUSSION

### Schlieren Photographs

Schlieren photographs of four-nozzle models are presented in figure 5 at ratios of nozzle-exit pressure to ambient pressure of about 19 for various nozzle extension ratios. The reflection of the exhaust-plume internal shocks from the plume impingement area is clearly visible. These reflected shocks are similar to those formed from an exhaust plume impinging on a plate placed perpendicular to the base, as reported in reference 8. The lines of impingement described earlier are also visible in some of the photographs and are indicated by white dots in figure 5(b). Since there is another set of nozzles directly behind those shown in the photographs, the lines of inpingement occur between the two sets of nozzles.

### Pressure Data

Since this investigation was intended to provide data for conditions of choked exhaust backflow within a cluster of nozzles, it was necessary to determine the extent of backflow choking within the various model configurations tested. The accepted criterion for a choked nozzle cluster is that further increases in the ratio of the nozzle-exit pressure to the ambient pressure $p_e/p_a$ (nozzle-exit pressure ratio) through increases in altitude produce no change in the flow properties or pressures within the cluster. Hence, one of the more sensitive measures of choking would be the ratio of the base-window pressure to the base-center pressure $p_w/p_c$, which should remain constant as the nozzle-exit pressure ratio continues to increase above the value required to initiate choking. Curves of $p_w/p_c$ plotted against $p_e/p_a$ are presented in figure 6 for the various nozzle extensions and nozzle spacings tested; a solid line has been drawn through the data symbols to indicate the conditions at which choking was thought to occur. Instead of a constant value at the choked conditions, these curves show a small decrease in $p_w/p_c$ with increases in $p_e/p_a$. Therefore, choking was considered to terminate when the slope of the curve showed a significant change as $p_e/p_a$ decreased. The small decrease in $p_w/p_c$ for choked conditions could be a result of partial choking at the window; this partial choking is most predominant for the case of extended nozzles for which a larger total-pressure gradient perpendicular to the base at the window might be expected.

The general trend of decreasing $p_w/p_e$ with decreasing nozzle extension for choked conditions does not include the zero nozzle extension. The abnormally high values of $p_w/p_c$ for $s/d_e = 0$ shown in figure 6(a) at $C_t/d_e = 0.35$ and $0.50$ are thought to be a result of the close proximity of the exhaust plumes to the base; this condition results in a flow component normal to the surface at the window. Consequently, some impact-pressure influence is felt in this region. These high pressures along the base at $s/d_e = 0$ may

also be seen from radial pressure distributions and are presented in the section entitled "Radial pressure distributions."

The ratio of the base-center pressure to the nozzle-exit pressure $p_c/p_e$ is shown in figure 7 as a function of nozzle-exit pressure ratio for the various model configurations tested. Again, a solid line is drawn through the data symbols to indicate the conditions at which choking is believed to exist. These curves are similar to curves of base-center pressure plotted against altitude normally presented in reports concerning backflow of exhaust gases. However, because of the Reynolds number effect introduced by varying the nozzle total pressure to alter the pressure ratio across the nozzles, it was necessary to use the ratio $p_c/p_e$ in order that it be comparable to other data. Where choking occurs (at other than zero nozzle extension), the curves for the four-nozzle cluster in figure 7(a) exhibit an apparent trend of rising and leveling off in the choked region. This rise in $p_c/p_e$ is believed to represent the transition zone between unchoked and choked backflow and results from increasing velocities at the window; eventually, sonic velocity is reached and the cluster is choked. A similar trend is reported in reference 2 in which altitude effects on the base pressure were considered. This trend is not as evident in the three-nozzle models of this investigation since the backflow was not as confined and little choking occurred.

Radial pressure distributions.- Radial pressure distributions along the base for those configurations for which choking or near choking was observed in figure 6 are presented in figures 8 to 12 in the form of the ratio of local base pressure to base-center pressure $p/p_c$ plotted against the nondimensional radius ratio $r/r_o$ from the center of the base. For each configuration three curves are presented corresponding to the maximum, intermediate, and minimum pressure ratios tested. Choked-backflow conditions are indicated by the flagged data symbols. In general, these pressure distributions decrease up to the window position ($r/r_o = 1.0$), at which point choking occurs, after which the pressure approaches ambient conditions, as is indicated by a dashed line. An exception can be seen in the curves for zero nozzle extension at the choked conditions for which a continued drop in pressure occurs beyond $r/r_o = 1.0$ to about $r/r_o = 1.4$. This continuing drop in pressure indicates that the backflow velocity is supersonic in this region. However, heat-transfer-coefficient data to be presented indicate that at most, supersonic backflow would exist only to about $r/r_o = 1.1$. It is believed that the close proximity of the exhaust plumes to the base results in some impact-pressure influence in the region of the window. This impact-pressure influence also can be observed in figure 6 when the abnormally high values of $p_w/p_c$ at the zero nozzle extension are considered.

Effect of number of nozzles.- Overall, the four-nozzle cluster yielded greater base pressures and a greater number of choked configurations than did the three-nozzle cluster. (See fig. 7.) The reason may be found by referring to figure 2, which reveals that for an extended-nozzle configuration the ratio of the base area within the nozzle cluster $A_n$ to the area between the nozzles $A_s$ is considerably smaller for the three-nozzle models. Since the base

area between the nozzles is an indication of the amount of plume area from which backflow can be derived, it is apparent that there is less backflow per unit window area for the three-nozzle models. Hence, the three-nozzle models are less restrictive and more difficult to choke.

Effect of nozzle extension.- The effect of nozzle extension on backflow pressure and choking may be seen in figure 7 which, at a constant value of $p_e/p_a$, shows a decrease in base-center pressure and backflow choking with increases in nozzle extension. This decrease in the base-center pressure is a result of total-pressure losses in the high-energy backflow either through mixing losses or by supersonic backflow followed by a normal shock standing off the center of the base. These pressure losses at the base center result in a lower average pressure gradient between the base center and window as the nozzle extension is increased; this trend may be seen by comparing the parts of figure 8. It may also be observed in figure 8(d) that the pressure distribution for $s/d_e = 1.5$ approaches that obtained from one-dimensional nozzle theory with a constant total pressure.

Figure 13(a) presents radial pressure distributions for the various nozzle extensions, replotted in the form of the local base pressure against the nondimensional radius ratio. This figure shows that as the nozzle extension increases, changes in pressure occur primarily in the center region of the base, up to about $r/r_o = 0.5$. It appears that the increased window area obtained through increases in nozzle extensions serves mainly to limit conditions of backflow choking and, for choked configurations, has little or no influence on the base pressures outside the base-center region. The upward displacement of the curve of $s/d_e = 0$ is believed to result from measuring impact pressure due to the close proximity of the exhaust plumes to the base.

Effect of nozzle spacing.- Increasing the spacing between nozzles influences the backflow by increasing the plume area and jet-boundary mixing length within the nozzle cluster. The increased mixing length permits an increase in backflow; however, at the same time the angle between impinging plumes decreases, tending to decrease the backflow. On the other hand, the window area is increased with increased nozzle spacing, causing the cluster to be less confining and yielding lower base pressures and less choking; this effect can be seen in figure 7 by comparing curves of various nozzle spacings. As a result, the majority of the choked data obtained in this investigation was at the smallest nozzle spacing $\left(C_t/d_e = 0.35\right)$.

It was found earlier that, neglecting zero-extension data, increasing the nozzle extension had the effect of decreasing the base pressure only in the center region of the base. This is not the case for increases in nozzle spacing. Figure 13(b) is a comparison of base pressure distributions for $C_t/d_e = 0.35$ and $0.50$ for $N = 4$ and reveals a general reduction in base pressure with increased nozzle spacing out to $r/r_o = 1.0$. This general reduction suggests a more uniform backflow from the jet plumes, resulting from the decreased angle between impinging plumes.

## Heat-Transfer Coefficients

Heat-transfer-coefficient distributions across the base are presented in figures 14 and 15 as the ratio of local- to base-center heat-transfer coefficient plotted against the nondimensional radius ratio. The data presented are for only those conditions at which choked backflow is suspected. Good agreement was obtained between data from the two sets of tests and is shown in figures 14(c) and 15(a); for the remaining parts of figures 14 and 15, an average heat-transfer coefficient was used when two data symbol points appeared at the same value of $r/r_o$. In general, the heat-transfer coefficients decreased from the base center outward, followed by a small rise in the window region where the flow is choked. For all the conditions considered, heat-transfer coefficients in the center region of the plate were as great as or greater than those in the region of the window. In some cases, particularly at $C_t/d_e = 0.35$ with $N = 4$ (figs. 14(a) and (b)), the cluster appears to be choked a little beyond $r/r_o = 1.0$, as is indicated by a high heat-transfer coefficient at $r/r_o = 1.1$. The heat-transfer-coefficient distributions varied with the test parameters in a manner similar to that of the pressure distributions presented earlier.

Effect of number of nozzles.- For similar test conditions the three-nozzle models yielded the lower base-center pressures and heat-transfer coefficients, which may be seen by comparing figures 14(a) and (b) with 15(a). A comparison of these figures also shows that the change in the level of the heat-transfer-coefficient distributions across the base is greater for the three-nozzle models than for the four-nozzle models when the nozzle extension is increased from $s/d_e = 0$ to 0.5. This greater change in pressure distribution for the three-nozzle models suggests a more uniform energy level of the exhaust backflow within these models having a nozzle extension.

Effect of nozzle extension.- The effect of increasing nozzle extension on the base-center heat-transfer coefficients and the radial heat-transfer-coefficient distributions is shown in figures 14(a) to (c) and 15(a). Each set of curves is for a constant value of $p_e/p_a$. In general, the configurations with the larger nozzle extensions yielded the lower base-center heat-transfer coefficients, as indicated in these figures. An exception to this is for the four-nozzle model at the zero nozzle extension which yields a higher base-center pressure but is accompanied by a heat-transfer coefficient equal to or less than that for the configurations with $s/d_e = 0.5$. (See figs. 14(a) to (c).) The low heat-transfer coefficients at the zero nozzle extension may be caused by a chilling of the highly confined backflow gases by the cooler base, causing the gas temperature in the base region to be cooler than the gases in the settling chamber. This chilling effect is discussed later.

A more even radial heat-transfer-coefficient distribution is also noted from these figures when the nozzle extension is increased and is attributed to increased losses in the core of high-energy backflow originating over the base center. As shown in the previous discussion on the effect of nozzle extension on base pressures, increasing nozzle extension resulted in decreasing base pressures primarily in the center region of the base. A similar effect may

be seen from the data in figures 14(a) and (b) if values of the heat-transfer coefficient ratios are multiplied by the center value $h_c$; this operation will show that for a nozzle extension other than zero the variation of heat-transfer coefficient with nozzle extension is primarily confined to $h_c$. This result suggests a well-defined core of high-energy backflow impinging on the center of the base. Supersonic backflow with a standing shock over the base center would be a logical explanation for the decreasing pressures and heat-transfer coefficients at the base center as the nozzle extension is increased. (See ref. 2.)

Effect of nozzle spacing.- The effect of nozzle spacing on heat-transfer coefficient for the four- and three-nozzle models is presented in figures 14(d) and 15(b), respectively. It can be seen from these figures that models having the smaller nozzle spacing yielded the higher base-center heat-transfer coefficients. There were some small variations in the radial heat-transfer-coefficient distributions at the different nozzle spacings, particularly in the region of the window; however, from these figures no definite pattern was found to occur.

Effect of nozzle pressure ratio.- A decrease in heat-transfer coefficient at the base center occurred with decreases in nozzle pressure ratio. (See figs. 14(e), 14(f), 15(c), and 15(d).) This decrease was brought about by a Reynolds number effect resulting from a varying of the nozzle total pressure when the ambient pressure was held constant. Theoretically, with choked flow at the windows, the base pressure and heat-transfer coefficient would remain constant with changes in nozzle pressure ratio if the total pressure remained constant and the ambient pressure decreased as would occur with increases in altitude. The heat-transfer-coefficient distributions showed no significant change with nozzle pressure ratio, indicating little change of the flow patterns within the nozzle cluster under the choked-backflow conditions.

## Effects of Backflow Characteristics on Base-Center Heat-Transfer Coefficients

In the preceding sections it was found that at a constant nozzle pressure ratio both the base-center pressure and heat-transfer coefficient were affected by nozzle extension and spacing. However, because of the strong dependency of heat transfer on local pressure, little has been learned concerning the effects of changes in the characteristics of the backflow. The effects of base-center pressure on the base-center heat-transfer coefficients are presented in figure 16(a) for the four-nozzle models. These curves show a straight-line relationship between the base-center heat-transfer coefficient and pressure, which is independent of choking. By considering a constant base-center pressure, the effects of nozzle extension on base-center heat-transfer coefficient may be seen. As shown in figure 16(a) at $C_t/d_e = 0.35$, the heat-transfer coefficient is constant at the two highest nozzle extensions but decreases as the nozzle extension approaches zero. The decrease in heat-transfer coefficient at the lower nozzle extensions is believed to be caused by a lowering of the average gas temperature by the base from a type of base chilling effect. This chilling

effect occurs under conditions for which the backflow is highly confined by small windows (e.g., see fig. 5 at $s/d_e = 0$), causing the mass flow rate of exhaust gases out of the cluster to be low.

In order to prove the concept of base chilling at low nozzle extensions, calculations were made to determine the temperature drop that might be expected to occur within the exhaust backflow. The temperature drop was calculated by equating the heat lost from the backflow gas to the heat gained by the base plate. The plane area $A_n$ was taken from figure 2, and the window area $A_w$ for the models with $s/d_e = 0$ was estimated from schlieren photographs. Sonic velocity was assumed to exist at the windows, and the heat flux at the base center was used. These calculations represent an approximation since some of the gases pass through the window without coming in contact with the base; also, a total-temperature gradient may be established within the exhaust gases along the base and depends on the circulation of the exhaust gases within the cluster. The calculated change of exhaust-gas temperature was subtracted from the original exhaust-gas total temperature, and this resultant temperature was used to determine the heat-transfer coefficients shown in figure 17. The change in heat-transfer coefficient (compare figs. 16 and 17) was negligible at the high nozzle extensions but was appreciable at the zero nozzle extension. The largest difference is approximately 10% to 15% and occurs for the configuration with $C_t/d_e = 0.35$, $s/d_e = 0$, and $N = 4$. Good agreement between the various nozzle extensions was obtained for the four-nozzle models of figure 17(a); this agreement indicated no effect of nozzle extension on curves relating the base-center heat-transfer coefficient to the base-center pressure. Similar corrections for base chilling applied to data for the three-nozzle models presented in figure 17(b) fail to show as good agreement between nozzle extensions as did the data for the four-nozzle models. It is believed that circulation effects within the three-nozzle models caused greater chilling of the backflow coming in contact with the center of the base so that corrections applied to the data for base chilling at the zero nozzle extension were not sufficient.

For comparative purposes, in figure 17(a) the curves of $C_t/d_e = 0.50$ and 0.75, represented by dashed lines, are included with the curve of $C_t/d_e = 0.35$. A comparison of these curves at a constant $p_c$ shows a small increase in heat-transfer coefficient with a decrease in nozzle spacing, with the greater change occurring between the two smaller nozzle spacings, represented by the curves $C_t/d_e = 0.35$ and $C_t/d_e = 0.50$. This trend suggests an alteration of the backflow to yield higher velocity gradients on the center portion of the base as the nozzle spacing decreases. It should be noted that according to accepted theory the heat-transfer coefficient at the stagnation point is directly proportional to the square root of the velocity gradient on the surface, extrapolated to conditions at the stagnation point.

Since good agreement was obtained between nozzle extensions for the four-nozzle models, the difference between the heat-transfer coefficients presented in figure 16(a) and the corrected data of figure 17(a) was used to calculate the amount of chilling present when the nozzles were flush with the base. The ratio of the decrease of the gas temperature on the base due to chilling $T_t - T_g$ to the difference between the stagnation and plate temperature $T_t - T_c$

was calculated and is presented in figure 18(a) as a function of nozzle spacing. The curve is extrapolated to a temperature ratio of 1.0 at $C_t/d_e = 0$ since the temperature of the gas would be expected to approach that of the base as the nozzle spacing and consequent outflux of backflow from the nozzle cluster approach zero. This figure suggests a reduction of heat flux to the base by going to a small nozzle spacing as a result of the decreased gas total temperature produced by base chilling. However, figure 18(b), which shows the percent increase of $h_c$ with decreases in nozzle spacing at a constant base pressure (data were arbitrarily picked at $p_c = 40$), indicates a sharp increase in base-center heat-transfer coefficient with decreases in spacing. At a constant nozzle pressure ratio an increase in pressure with decreasing nozzle spacing may be observed in figure 18(c); this increase in pressure produces an increase in heat-transfer coefficient. (See fig. 17.) Therefore, for a given nozzle pressure ratio, reducing the nozzle spacing reduces the backflow-gas temperature but increases the base-center heat-transfer coefficient. Data from the curves of figure 18 indicate that by reducing the spacing ratio from 0.75 to 0.35 on a model with four nozzles flush with the base, a 10% reduction in the difference between the backflow and base temperatures might be expected, whereas the heat-transfer coefficient is increased by about 65% through the combined effects shown in figures 18(b) and (c), causing the heat flux into the base to be increased substantially.

### Summary of Base-Center Heat-Transfer-Coefficient Data

A summary of the base-center heat-transfer coefficients of figure 16 are presented in figure 19 in the form of Stanton number related to Reynolds number. The Stanton number for this investigation was based on a sonic velocity at the window and conditions at the center of the base; that is, $N_{St} = \left(\frac{h}{\rho c}\right)_c \left(\frac{1}{a}\right)_w$. The Reynolds number was based on the nozzle-exit velocity, nozzle-exit diameter, and conditions at the center of the base: $R = \left(\frac{\rho}{\mu}\right)_c (Vd)_e$. For simplicity, an average total temperature of 120° F was used.

## SUMMARY OF RESULTS

From a general base heating investigation on rocket-base configurations containing clusters of three and four sonic nozzles, conducted to determine local heat-transfer coefficients and pressures due to backflowing exhaust gases choked within the nozzle cluster, the following results were obtained:

1. The highest pressures and heat-transfer coefficients were found at the center region of the base, with a second but smaller rise in heat-transfer coefficient occurring between adjacent nozzles.

2. Increasing nozzle extension resulted in decreased pressures and heat-transfer coefficients primarily at the center of the base. This effect produced more uniform pressure and heat-transfer-coefficient distributions with increases in nozzle extension.

3. Pressures and heat-transfer coefficients across the base were decreased by increasing the nozzle spacing and decreasing the nozzle pressure; the more severe conditions occurred for the four-nozzle models.

4. At a common base-center pressure on models containing four nozzles, decreases in the nozzle spacing increased the base-center heat-transfer coefficient, whereas decreases in the nozzle extension produced decreases in the base-center heat-transfer coefficient only at the lower nozzle extensions. The decrease in heat-transfer coefficient with decreasing nozzle extension is attributed to a chilling of the backflow gases within the nozzle cluster such that, based on a corrected gas temperature, curves of heat-transfer coefficient plotted against pressure at the center of the base is independent of nozzle extension.

Langley Research Center,
National Aeronautics and Space Administration,
Langley Station, Hampton, Va., April 29, 1965.

## REFERENCES


1. Goethert, B. H.: Base Flow Characteristics of Missiles With Cluster-Rocket Exhausts. Paper No. 60-89, Inst. Aero. Sci., June-July 1960.

2. Marion, E. D.; Daniels, D. J.; Herstine, G. L.; and Burge, G. W.: Exhaust Reversal From Cluster Nozzles - A New Flow Model. [Preprint] 2706-62, Am. Rocket Soc., Nov. 1962.

3. Musial, Norman T.; and Ward, James J.: Base Flow Characteristics for Several Four-Clustered Rocket Configurations at Mach Numbers From 2.0 to 3.5. NASA TN D-1093, 1961.

4. Charczenko, Nickolai; and Hayes, Clyde: Jet Effects at Supersonic Speeds on Base and Afterbody Pressures of a Missile Model Having Single and Multiple Jets. NASA TN D-2046, 1963.

5. Dawson, John G., Jr.: An Investigation of Base Heating on a 5.47-Percent-Scale Model Saturn SA-1 Booster Afterbody at Mach Numbers 1.63 and 3.07. AEDC-TDR-62-9, U.S. Air Force, Jan. 1962.

6. Kennedy, T. L.; and Lowry, J. F.: An Investigation of Base Heating on a 5.47-Percent Scale Model of the Saturn S-1 Booster at Transonic Mach Numbers. AEDC-TN-61-106, U.S. Air Force, Aug. 1961.

7. Schneider, P. J.: Temperature Response Charts. John Wiley & Sons, Inc., 1963, p. 119.

8. Vick, Allen R.; and Andrews, Earl H., Jr.: An Experimental Investigation of Highly Underexpanded Free Jets Impinging Upon a Parallel Flat Surface. NASA TN D-2326, 1964.

TABLE I.- LOCATIONS OF BASE-PLATE INSTRUMENTATION IN FORM OF $r/r_o$ FOR FIRST SET OF TESTS

(a) Thermocouples

| Number of nozzles, N | Nozzle spacing | | Thermocouple location, $r/r_o$ | | | | | | | | | |
|---|---|---|---|---|---|---|---|---|---|---|---|---|
| | $C_t/d_e$ | $r_o$ | 1 | 2 | 3 | 4 | 5 | 6 | 7 | 8 | 9 | 10 |
| 4 | 0.35 | 0.506 | 0.60 | 1.00 | 1.40 | 1.79 | | 0.41 | 0.80 | 1.20 | 1.59 | 1.99 |
| | .50 | .562 | .64 | 1.00 | 1.36 | 1.71 | | .47 | .82 | 1.18 | 1.53 | 1.89 |
| | .75 | .656 | .39 | .70 | 1.00 | 1.31 | 1.61 | .54 | .85 | 1.15 | 1.46 | 1.76 |
| 3 | 0.35 | 0.292 | 0.49 | 1.00 | 1.68 | 2.37 | 3.06 | 0.68 | 1.37 | 2.06 | 2.74 | |
| | .50 | .325 | .54 | ↓ | 1.62 | 2.23 | 2.85 | .92 | 1.85 | 2.77 | 3.69 | |
| | .75 | .379 | .47 | ↓ | 1.79 | 2.58 | 3.38 | .79 | 1.58 | 2.37 | 3.16 | |

(b) Pressure orifices

| Number of nozzles, N | Nozzle spacing | | Pressure-orifice location, $r/r_o$ | | | | | | | |
|---|---|---|---|---|---|---|---|---|---|---|
| | $C_t/d_e$ | $r_o$ | 1 | 2 | 3 | 4 | 5 | 6 | 7 | 8 |
| 4 | 0.35 | 0.506 | 0 | 0.60 | 1.00 | 1.40 | 1.79 | 2.19 | 2.58 | |
| | .50 | .562 | ↓ | .64 | 1.00 | 1.36 | 1.71 | 2.07 | 2.42 | |
| | .75 | .656 | ↓ | .39 | .70 | 1.00 | 1.31 | 1.61 | 1.91 | 2.22 |
| 3 | 0.35 | 0.292 | 0 | 0.49 | 1.00 | 1.51 | 2.03 | 2.54 | 3.06 | |
| | .50 | .325 | ↓ | .54 | ↓ | 1.46 | 1.92 | 2.54 | 3.15 | |
| | .75 | .379 | ↓ | .47 | ↓ | 1.53 | 2.06 | 2.58 | | |

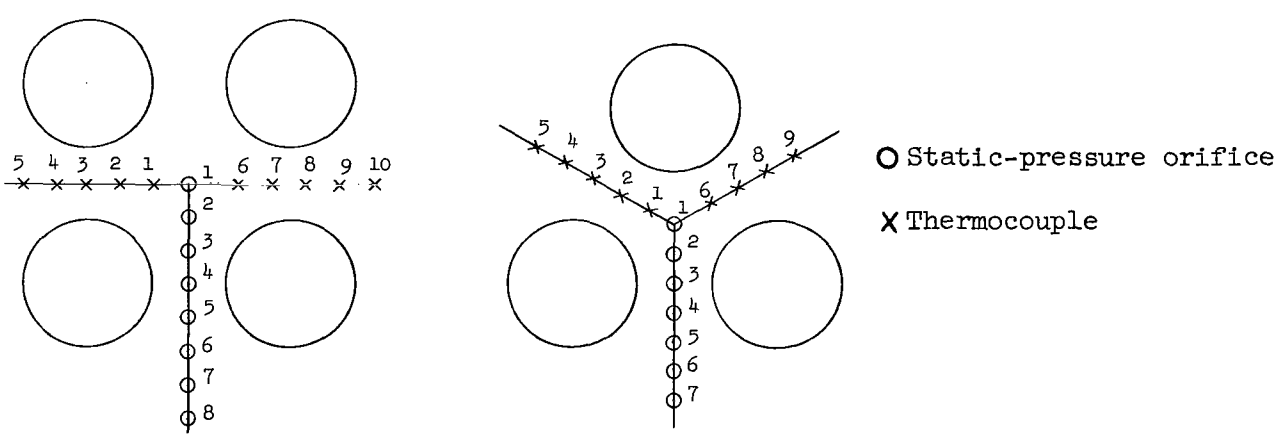

TABLE II.- LOCATIONS OF BASE-PLATE INSTRUMENTATION IN FORM OF $r/r_o$ FOR SECOND SET OF TESTS

(a) Thermocouples

| Number of nozzles, N | Nozzle spacing | | Thermocouple location, $r/r_o$ | | | | | | | | |
|---|---|---|---|---|---|---|---|---|---|---|---|
| | $C_t/d_e$ | $r_o$ | 1 | 2 | 3 | 4 | 5 | 6 | 7 | 8 | 9 |
| 4 | 0.35 | 0.506 | 0 | 0.41 | 0.80 | 1.20 | 0.90 | 1.10 | 0.21 | 0.60 | 1.00 |
| | .50 | .562 | ↓ | .47 | .82 | 1.18 | .91 | 1.09 | .29 | .64 | ↓ |
| | .75 | .656 | ↓ | .24 | .54 | 1.15 | .92 | 1.08 | .39 | .70 | ↓ |
| 3 | 0.35 | 0.292 | 0 | 0.49 | 1.00 | 0.31 | 0.83 | 1.17 | | | |
| | .50 | .325 | ↓ | .54 | ↓ | .31 | .85 | 1.15 | | | |
| | .75 | .379 | ↓ | .47 | ↓ | .26 | .87 | 1.13 | | | |

(b) Pressure orifices

| Number of nozzles, N | Nozzle spacing | | Pressure-orifice location, $r/r_o$ | | |
|---|---|---|---|---|---|
| | $C_t/d_e$ | $r_o$ | 1 | 2 | 3 |
| 4 | 0.35 | 0.506 | 0.60 | 1.00 | 1.40 |
| | .50 | .562 | .64 | 1.00 | 1.36 |
| | .75 | .656 | .39 | .70 | 1.00 |
| 3 | 0.35 | 0.292 | 1.00 | 1.51 | |
| | .50 | .325 | ↓ | 1.46 | |
| | .75 | .379 | ↓ | 1.53 | |

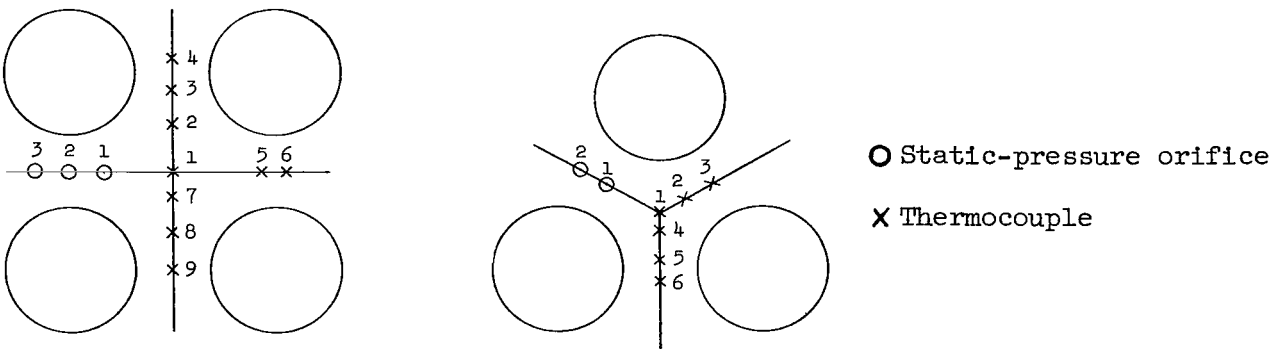

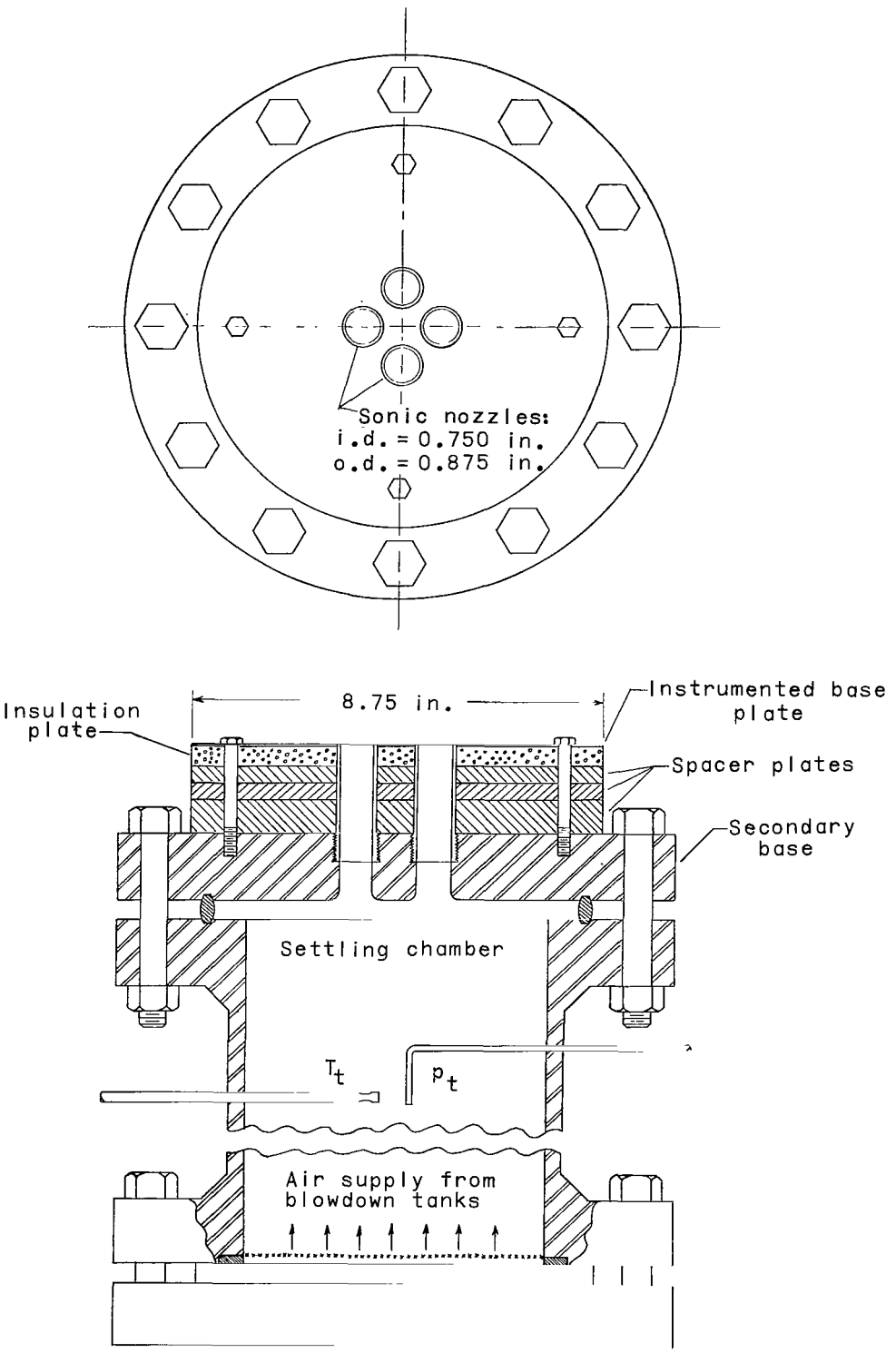


Figure 1.- Cutaway view of test apparatus.

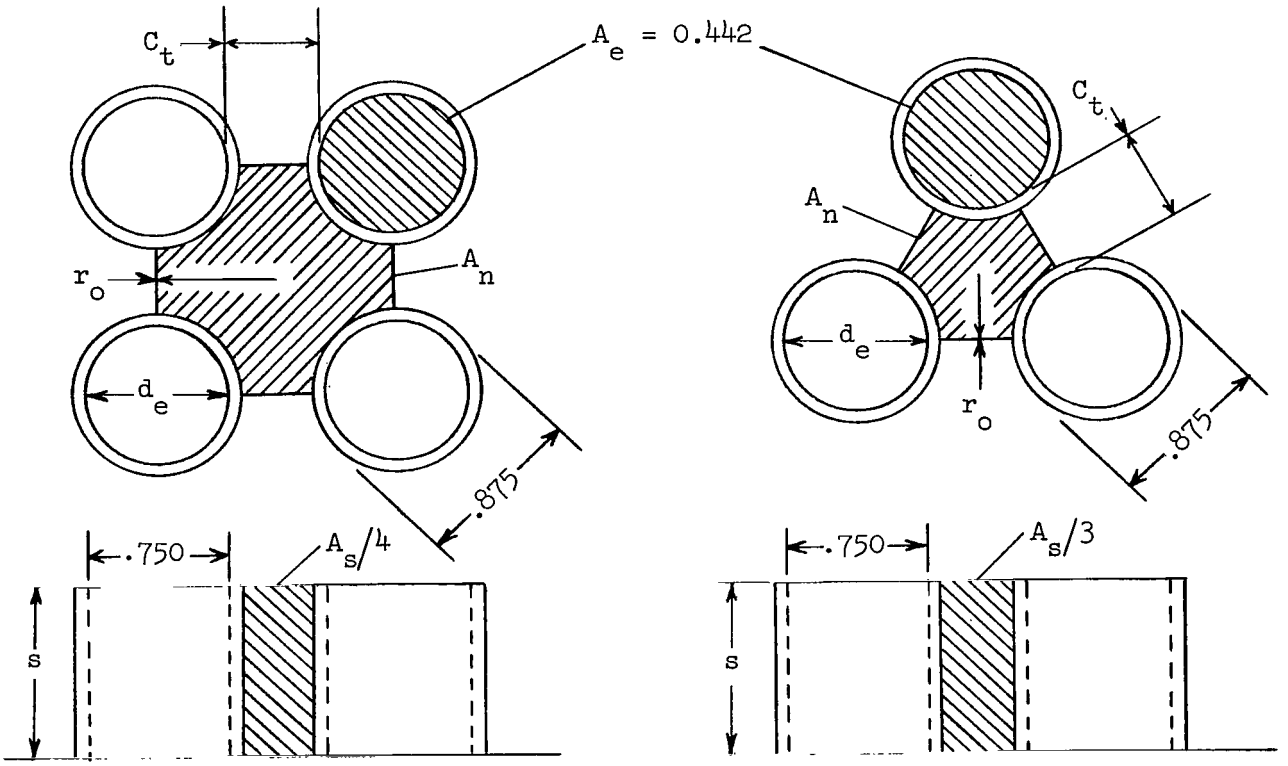


| Number of nozzles, N | $C_t$ | $r_o$ | $A_n$ | Parameter: $A_s$ for values of s of - | | | |
|---|---|---|---|---|---|---|---|
| | | | | 0 | 0.375 | 0.750 | 1.125 |
| 4 | 0.262 | 0.506 | 0.421 | 0 | 0.204 | 0.412 | 0.618 |
| | .375 | .562 | .660 | ↓ | .372 | .748 | 1.120 |
| | .562 | .656 | 1.118 | ↓ | .656 | 1.312 | 1.968 |
| 3 | 0.262 | 0.292 | 0.142 | 0 | 0.153 | 0.309 | 0.462 |
| | .375 | .325 | .246 | ↓ | .281 | .564 | .843 |
| | .562 | .379 | .444 | ↓ | .492 | .984 | 1.476 |

Figure 2.- Geometric parameters used in investigation.

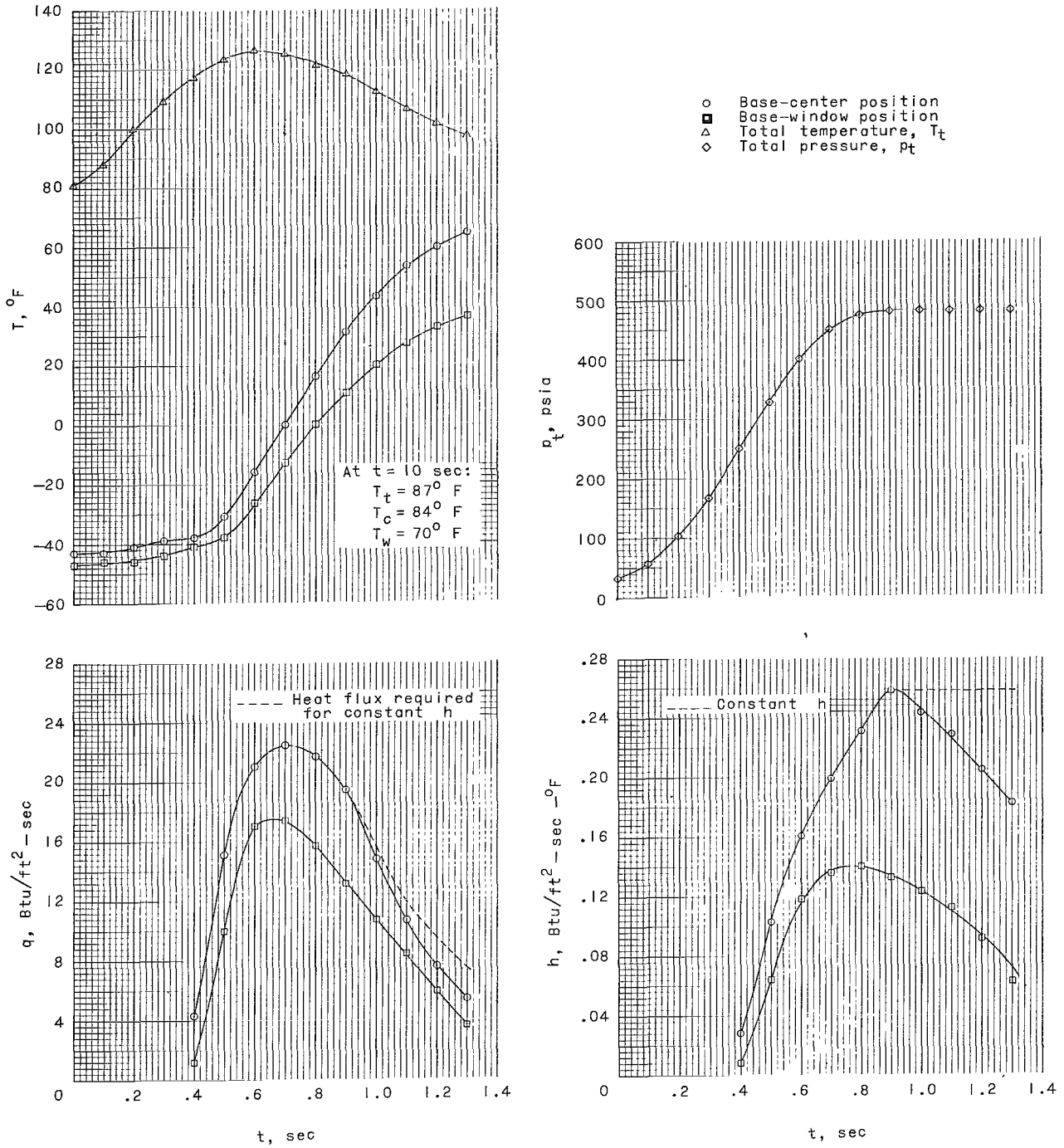


Figure 3.- Typical time histories of temperature, heat flux, and heat-transfer coefficient for $C_t/d_e = 0.35$, $s/d_e = 0.5$, $N = 4$, $p_e/p_a = 17.1$.

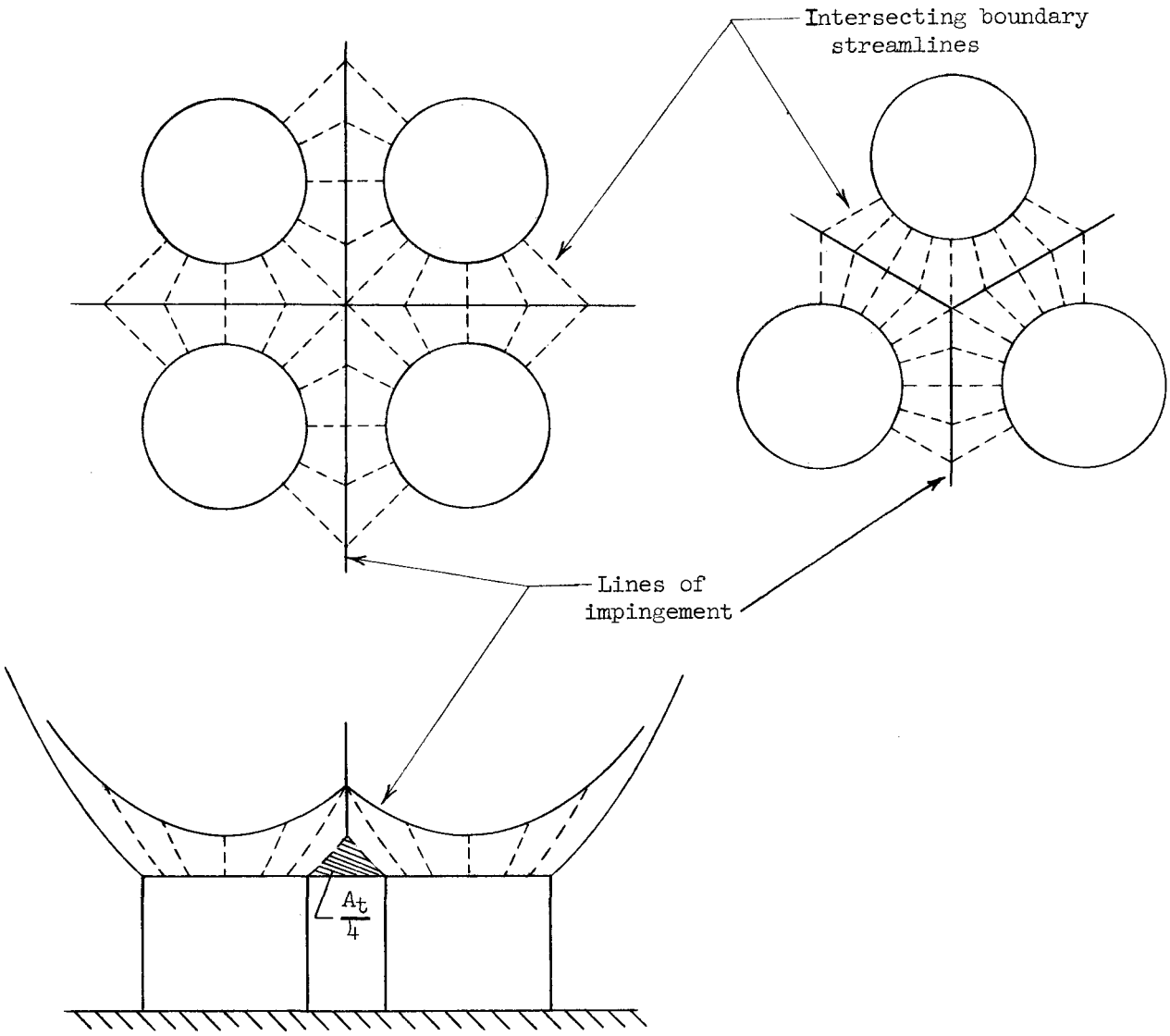


Figure 4.- Diagrams of three- and four-nozzle clusters with impinging exhaust plumes.

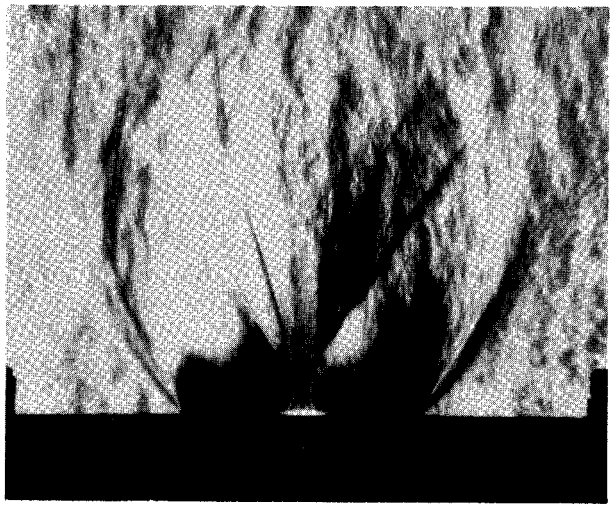

$s/d_e = 0$

$p_e/p_a = 18.6$

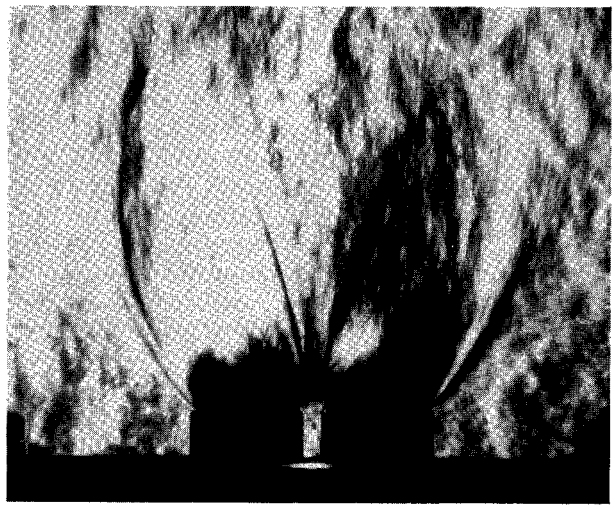

$s/d_e = 0.5$

$p_e/p_a = 18.9$

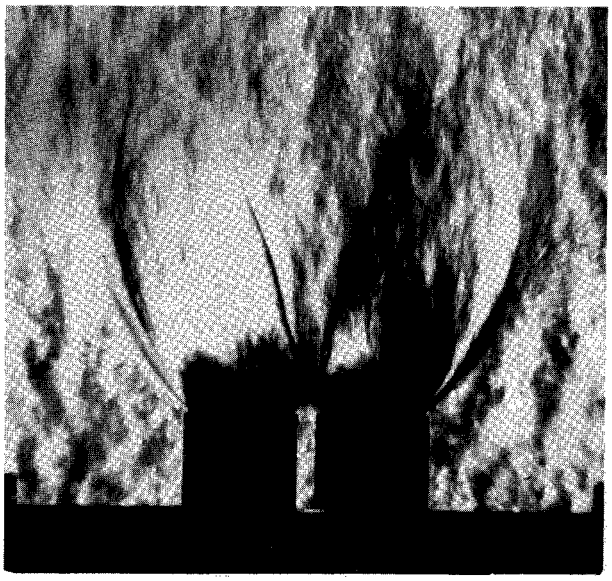

$s/d_e = 1.0$

$p_e/p_a = 19.2$

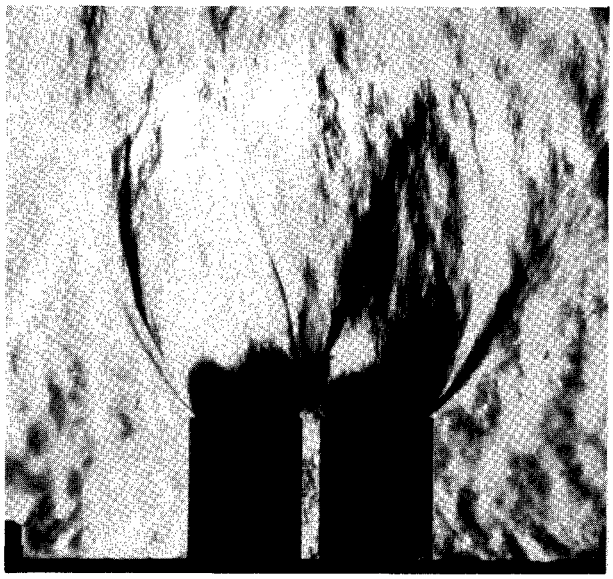

$s/d_e = 1.5$

$p_e/p_a = 18.7$

(a) $C_t/d_e = 0.35$.

Figure 5.- Schlieren photographs of four-nozzle model.

L-65-105

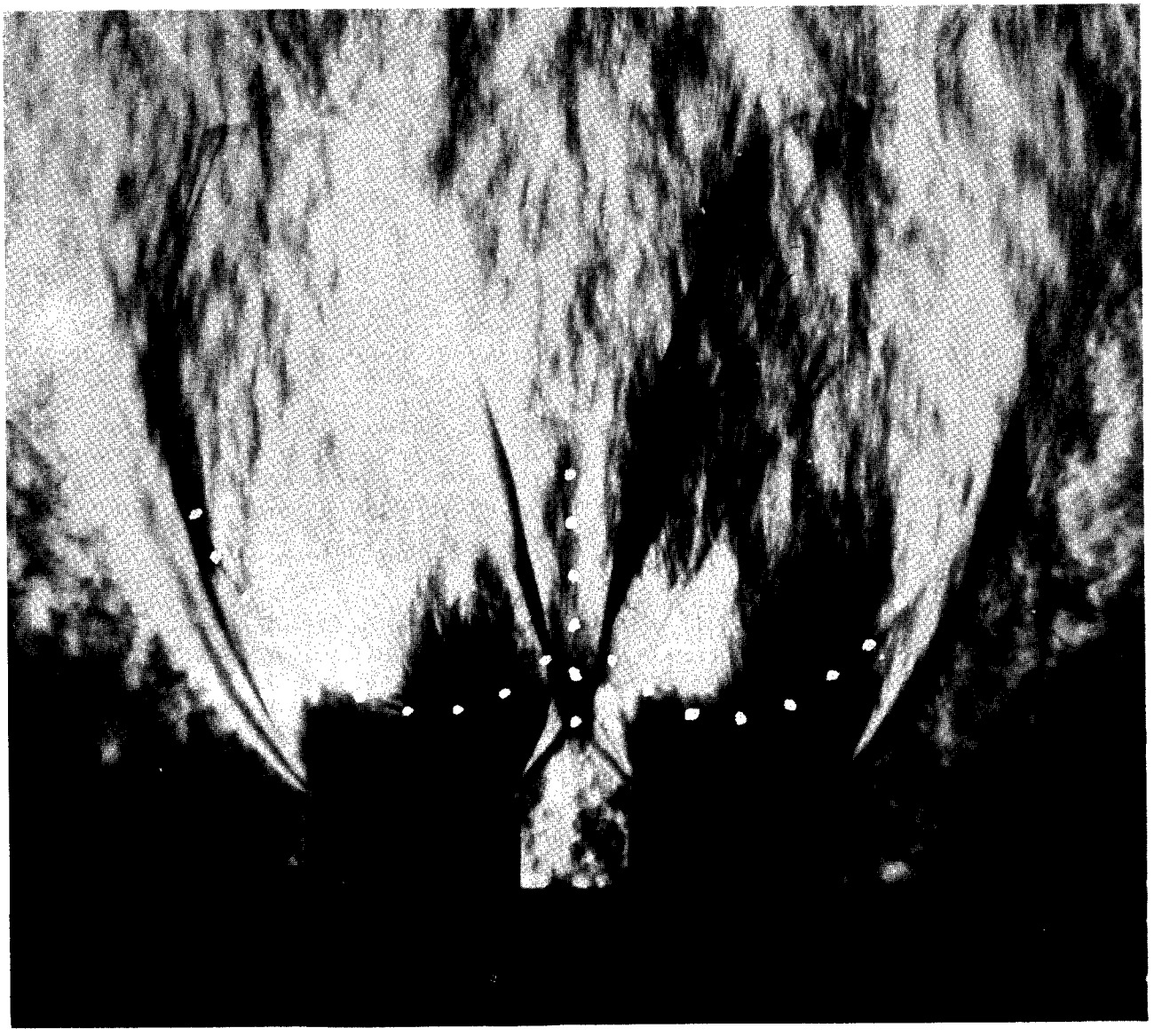

$s/d_e = 0.5$

$p_e/p_a = 18.7$

(b) $C_t/d_e = 0.75$. (Dots indicate lines of impingement.) L-65-106

Figure 5. - Concluded.

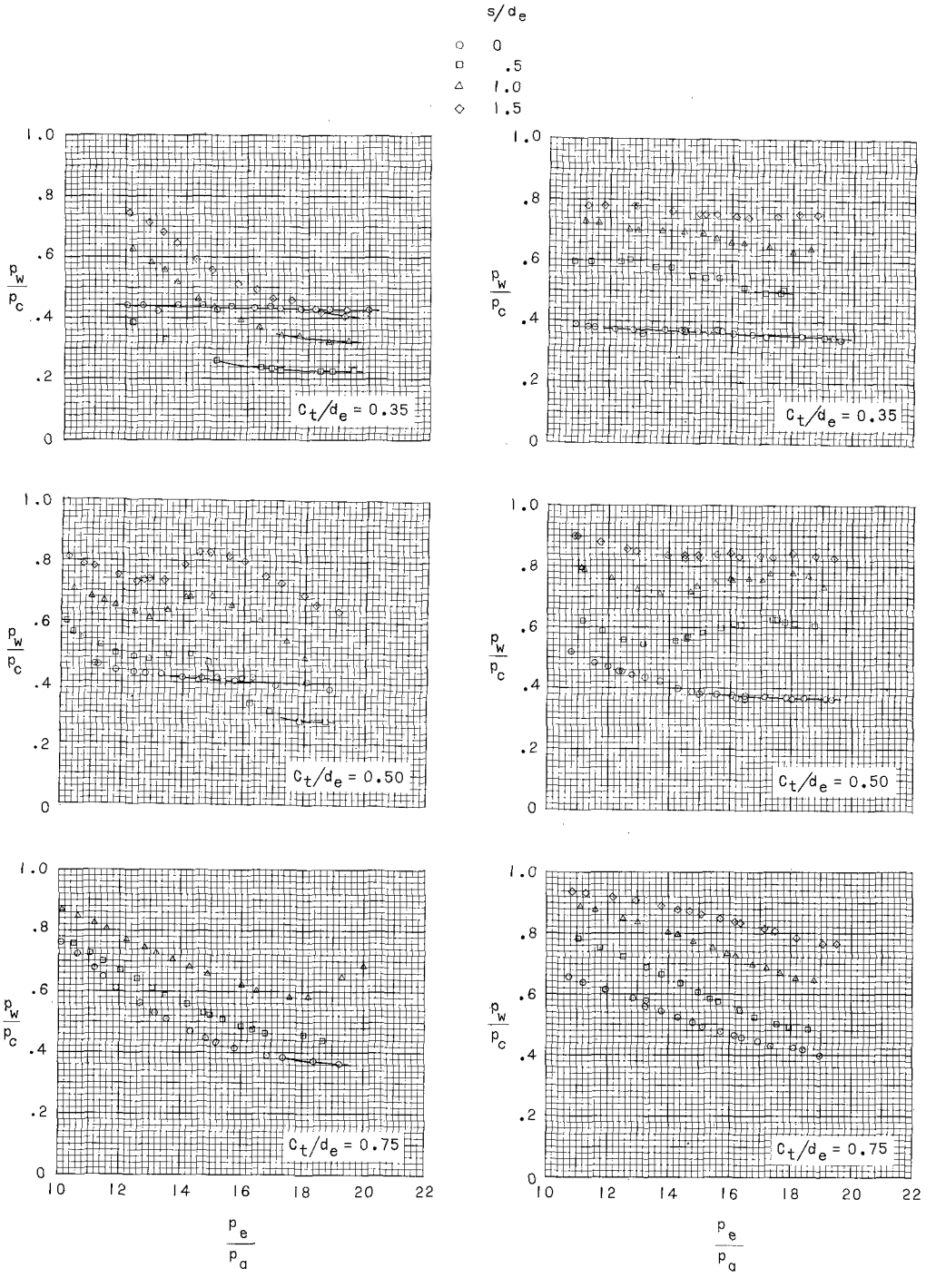


(a) N = 4. (b) N = 3.

Figure 6.- Variation of ratio of base-window pressure to base-center pressure with nozzle-exit pressure ratio. (Solid lines denote choked conditions.)

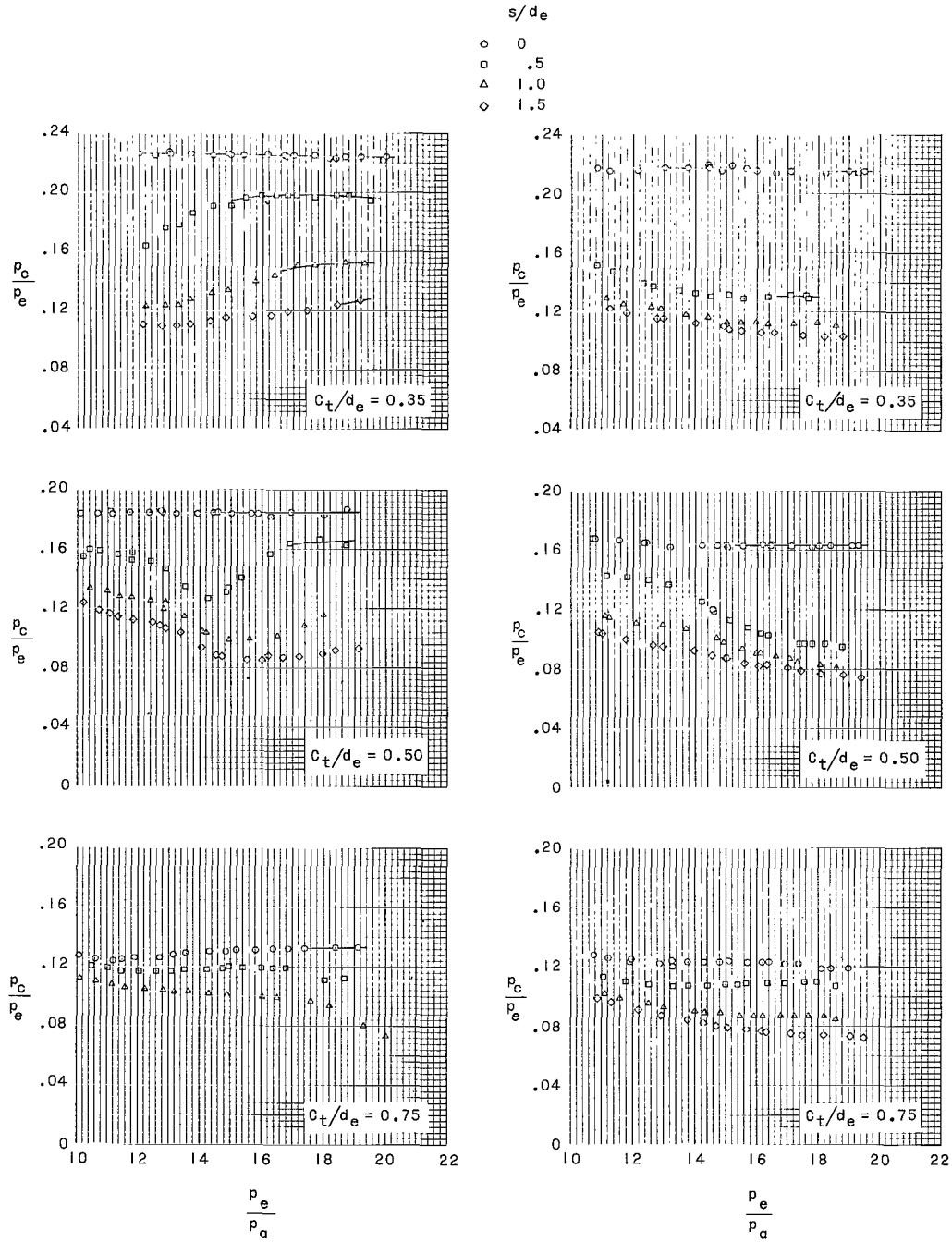


Figure 7.- Variation of ratio of base-center pressure to nozzle-exit pressure with nozzle-exit pressure ratio. (Solid lines denote choked conditions.)

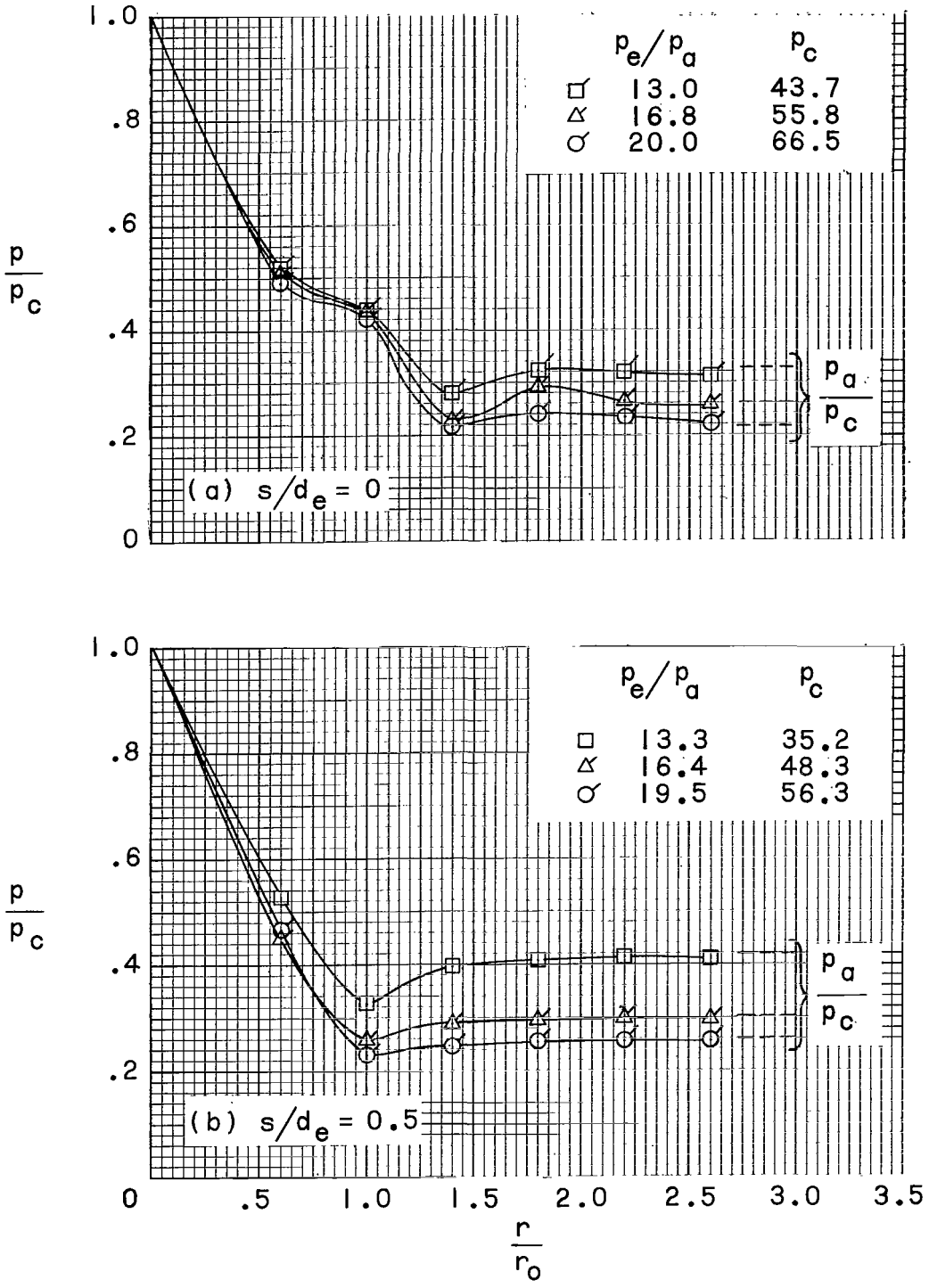


Figure 8.- Radial pressure distributions across base plate for $C_t/d_e = 0.35$ and $N = 4$.
(Flagged data symbols indicate conditions of choked backflow.)

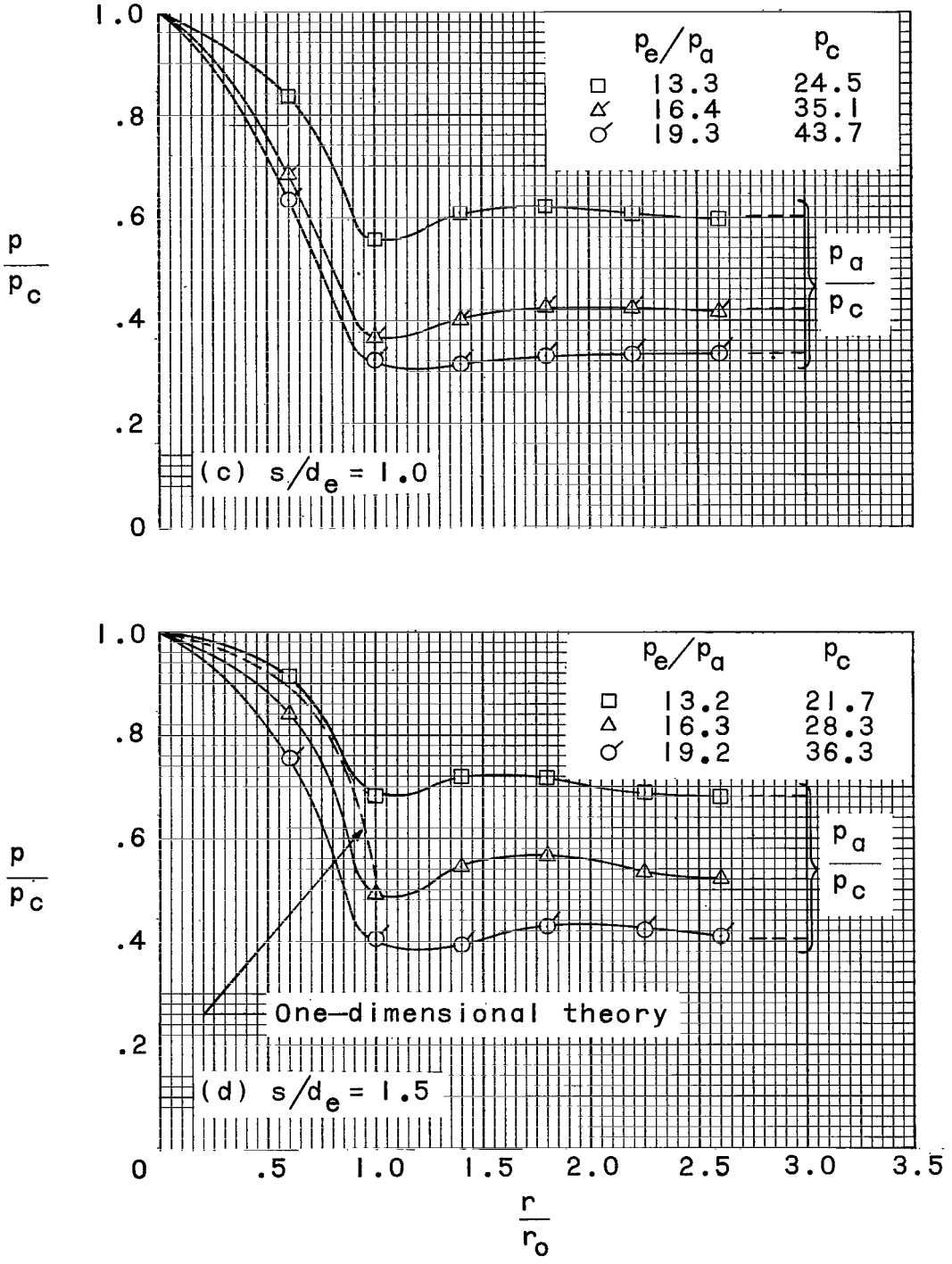


Figure 8.- Concluded.

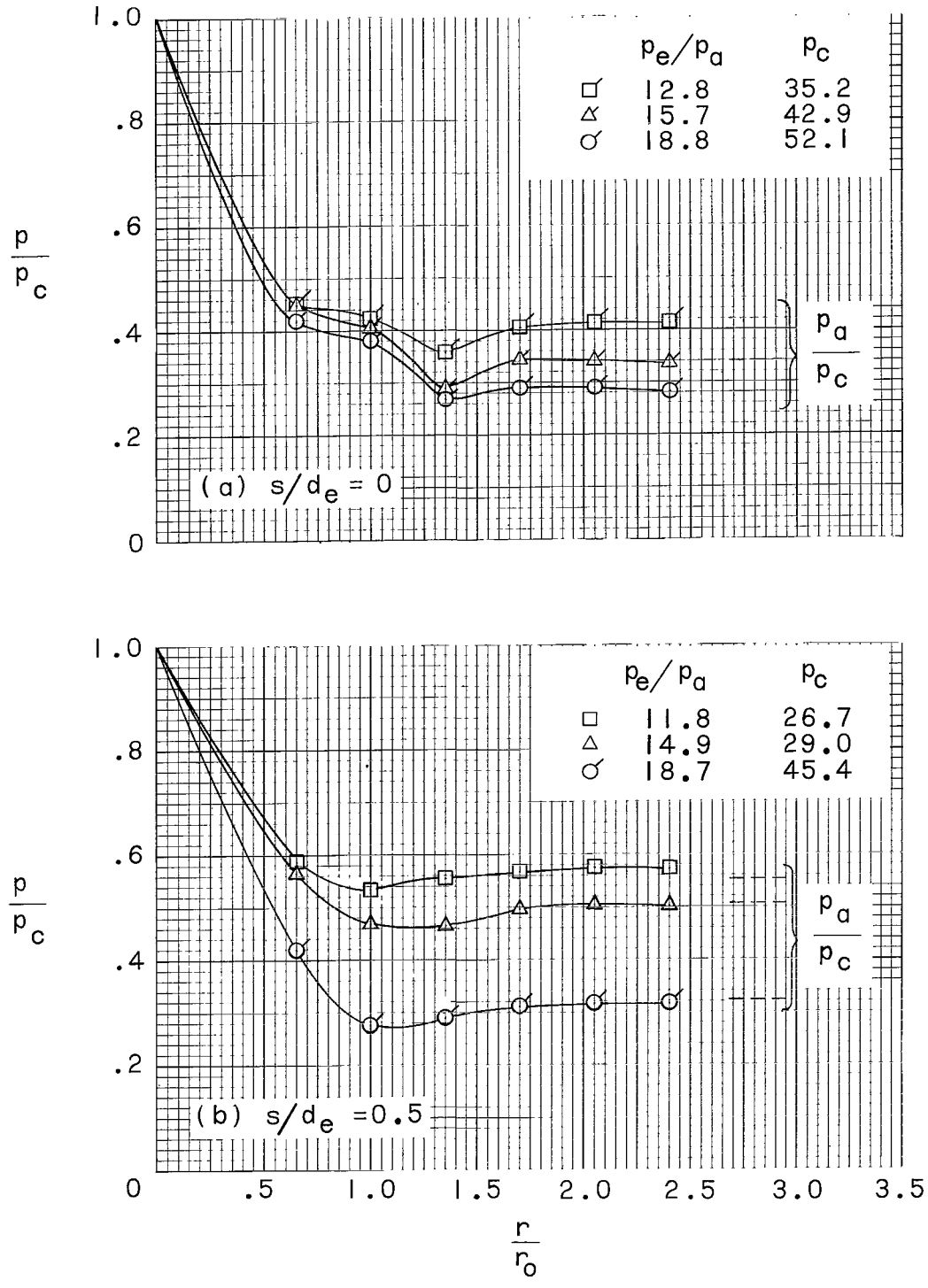


Figure 9.- Radial pressure distributions across base plate for $C_t/d_e = 0.50$ and $N = 4$.
(Flagged data symbols indicate conditions of choked backflow.)

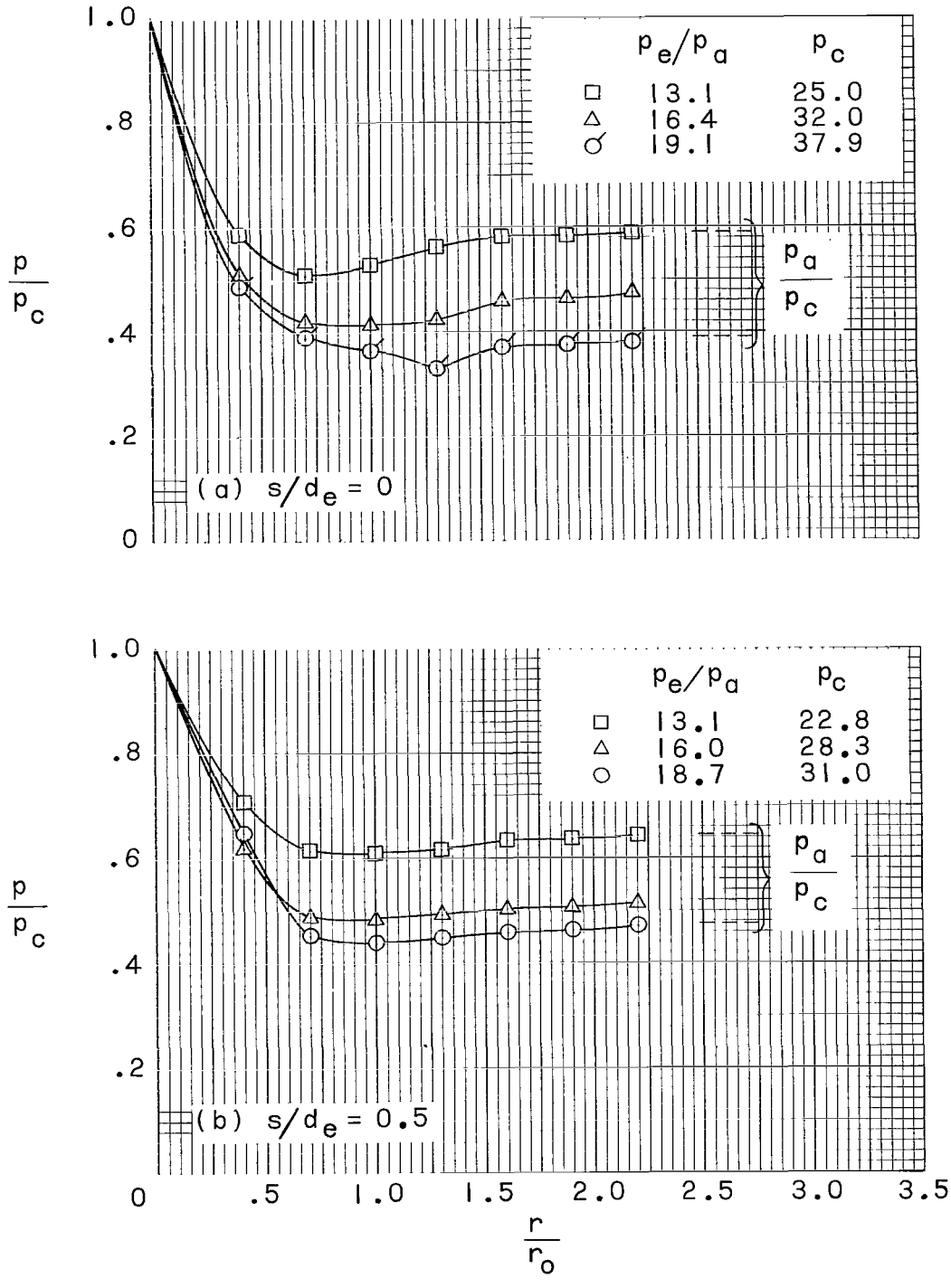


Figure 10.- Radial pressure distributions across base plate for $C_t/d_e = 0.75$ and $N = 4$.
(Flagged data symbols indicate conditions of choked backflow.)

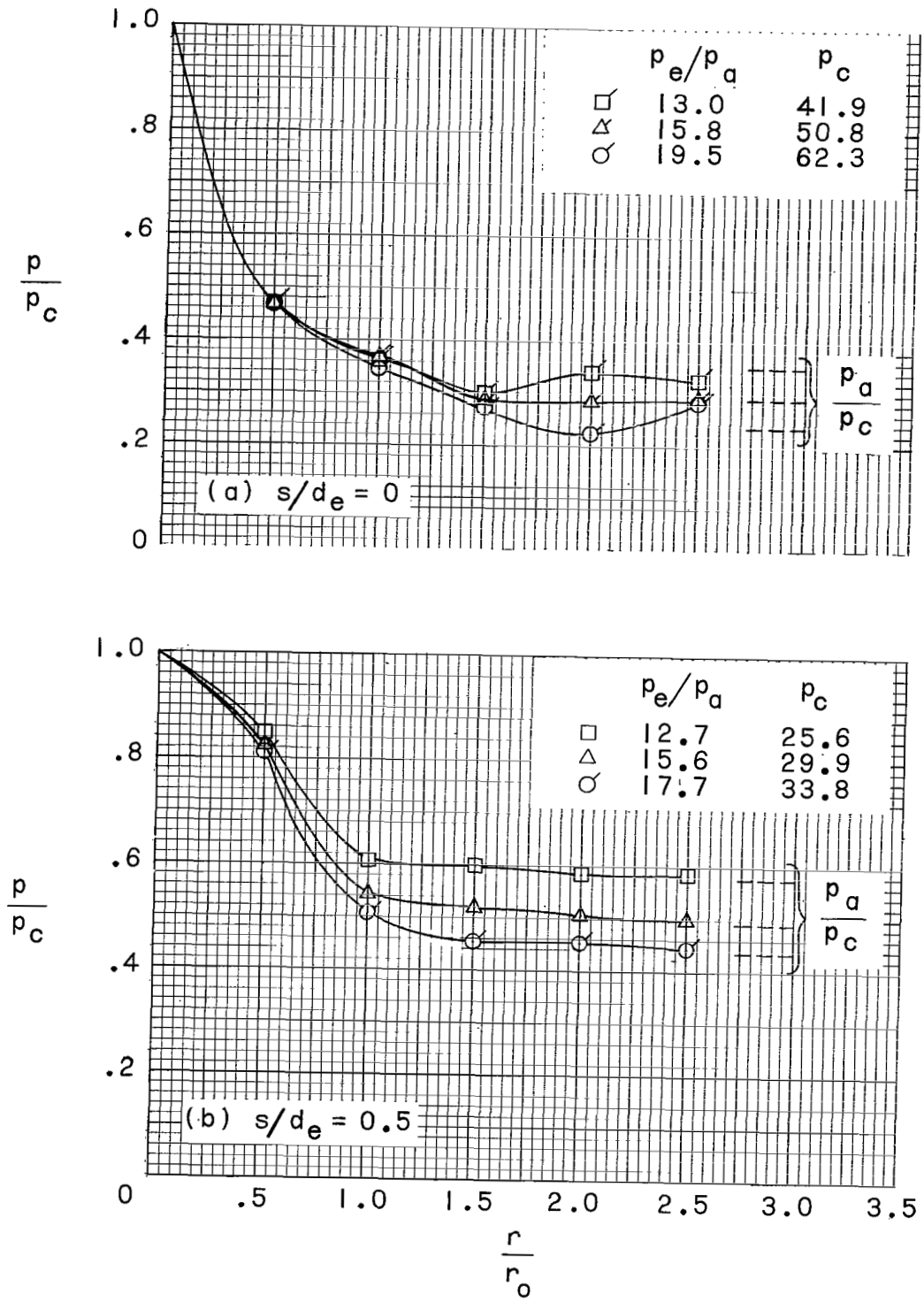


Figure 11.- Radial pressure distributions across base plate for $C_t/d_e = 0.35$ and $N = 3$. (Flagged data symbols indicate conditions of choked backflow.)

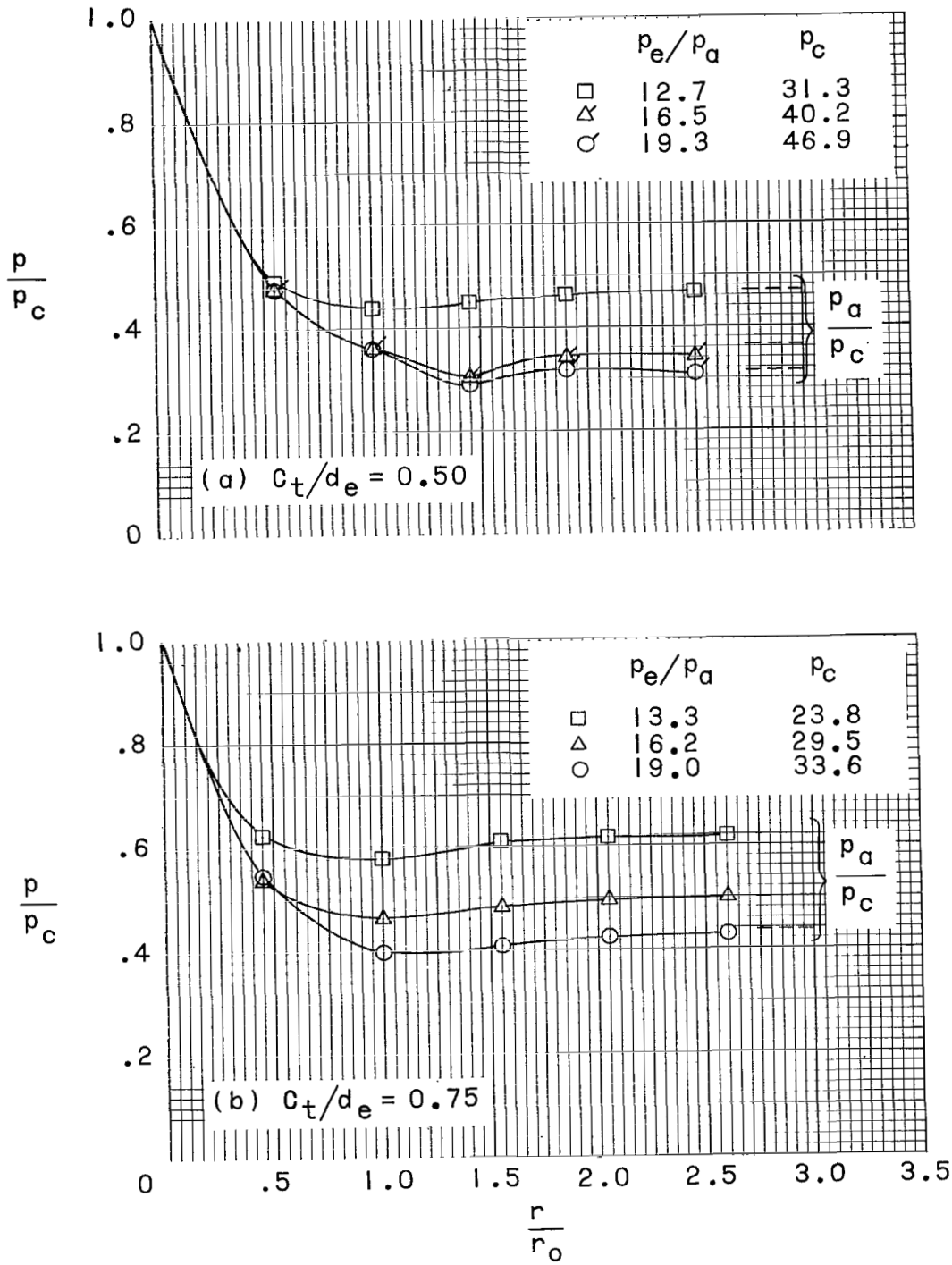


Figure 12.- Radial pressure distributions across base plate for $s/d_e = 0$ and $N = 3$. (Flagged data symbols indicate conditions of choked backflow.)

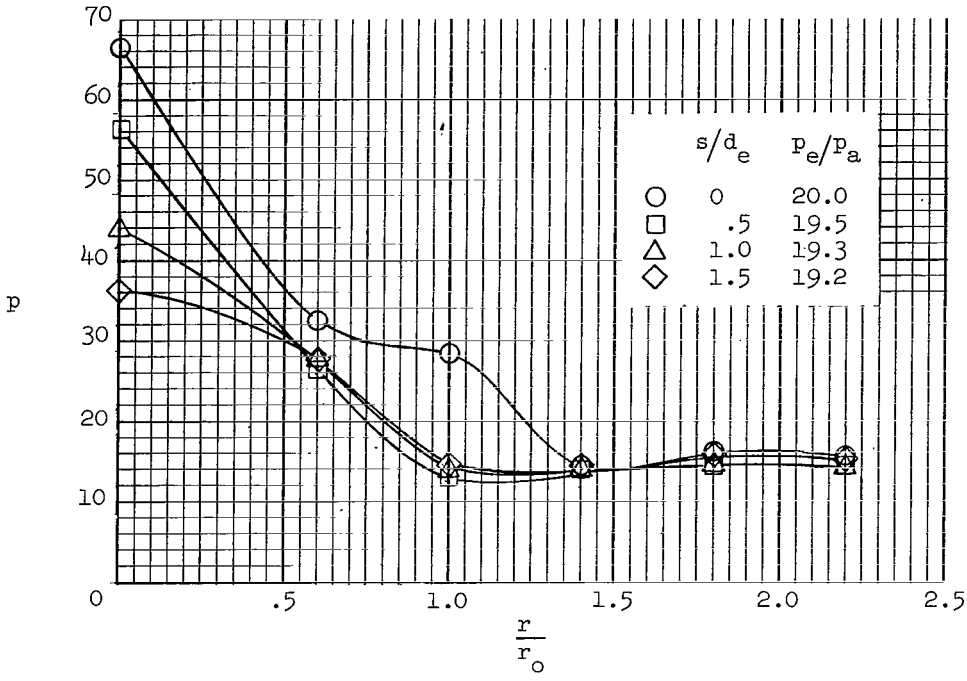


(a) Variable nozzle extension for $C_t/d_e = 0.35$.

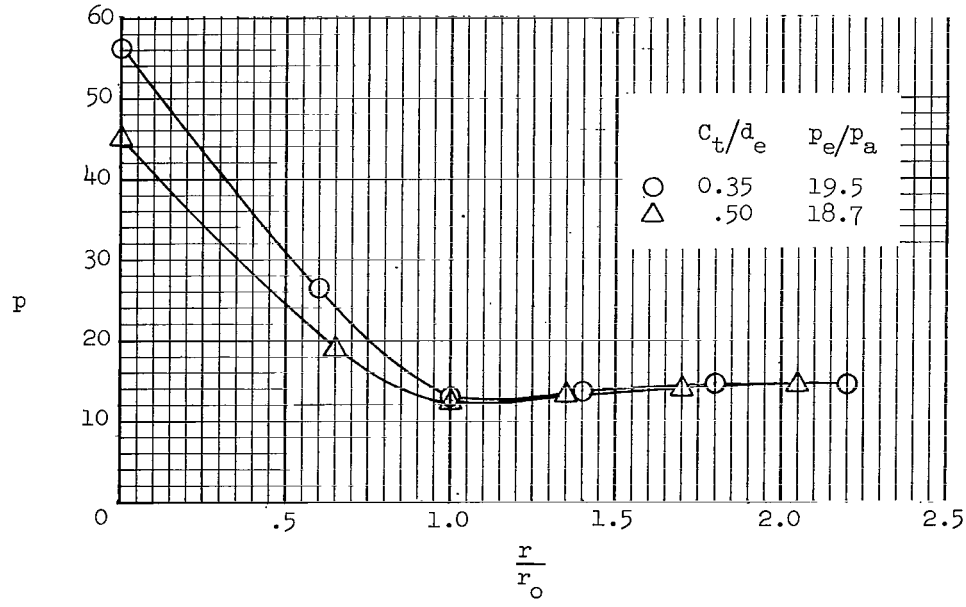


(b) Variable nozzle spacing for $s/d_e = 0.5$.

Figure 13.- Variation of local base pressure with changes in nozzle extension and nozzle spacing for N = 4.

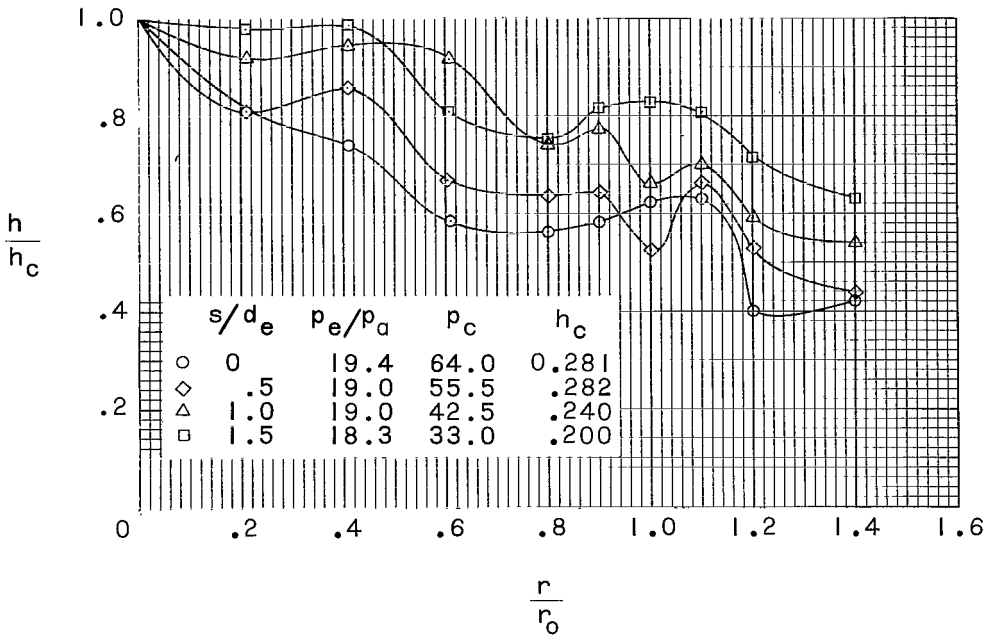


(a) Variable nozzle extension for $C_t/d_e = 0.35$.

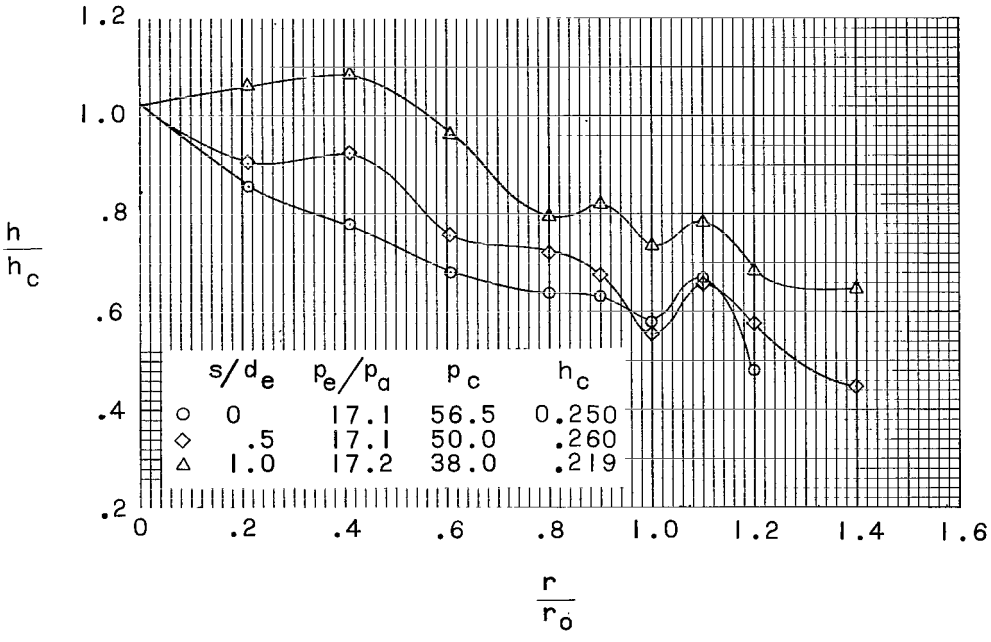


(b) Variable nozzle extension for $C_t/d_e = 0.35$.

Figure 14.- Radial heat-transfer-coefficient distribution for choked backflow at N = 4.

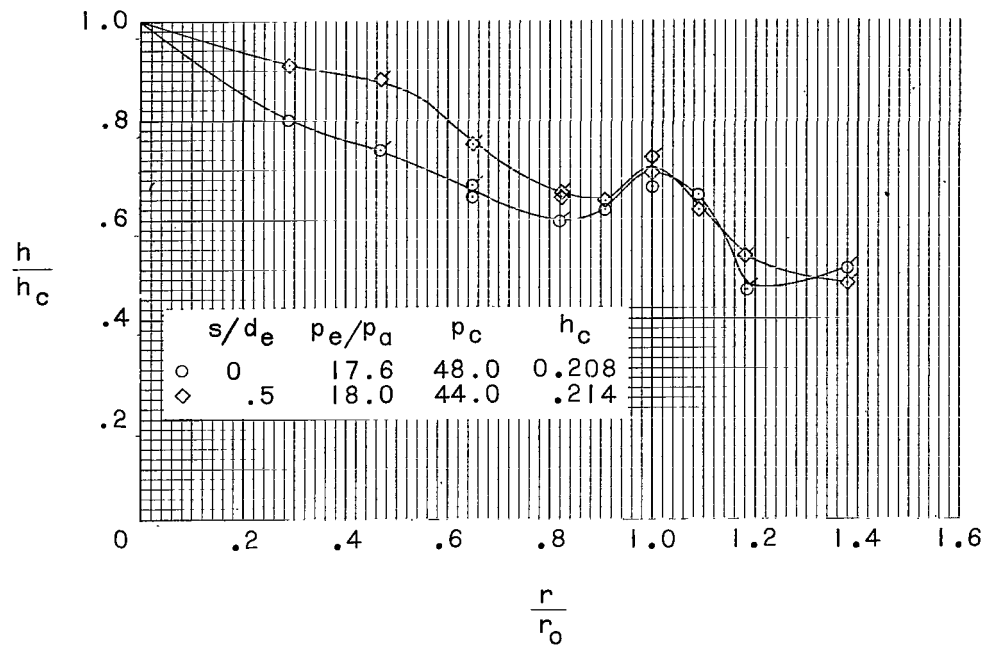


(c) Variable nozzle extension for $C_t/d_e = 0.50$. (Flagged data symbols represent data from first set of tests.)

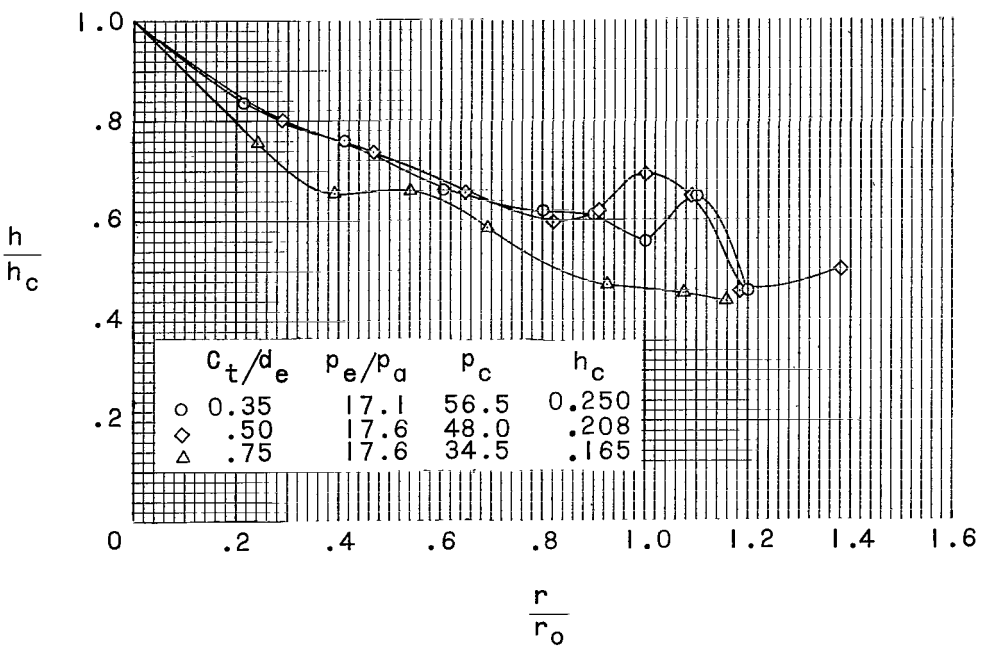


(d) Variable nozzle spacing for $s/d_e = 0$.

Figure 14.- Continued.

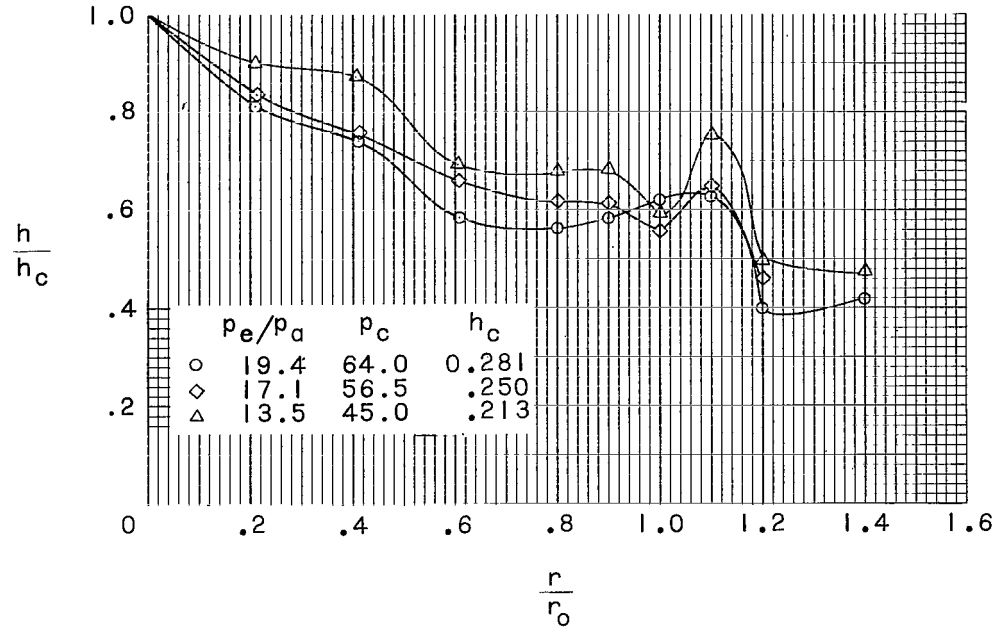


(e) Variable nozzle pressure ratio for $C_t/d_e = 0.35$ and $s/d_e = 0$.

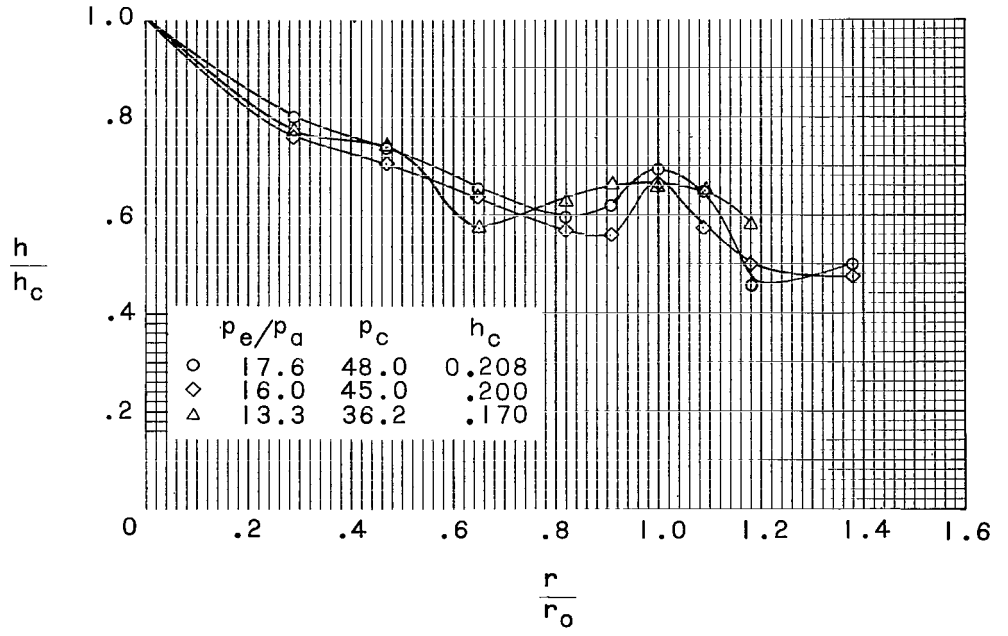


(f) Variable nozzle pressure ratio for $C_t/d_e = 0.50$ and $s/d_e = 0$.

Figure 14.- Concluded.

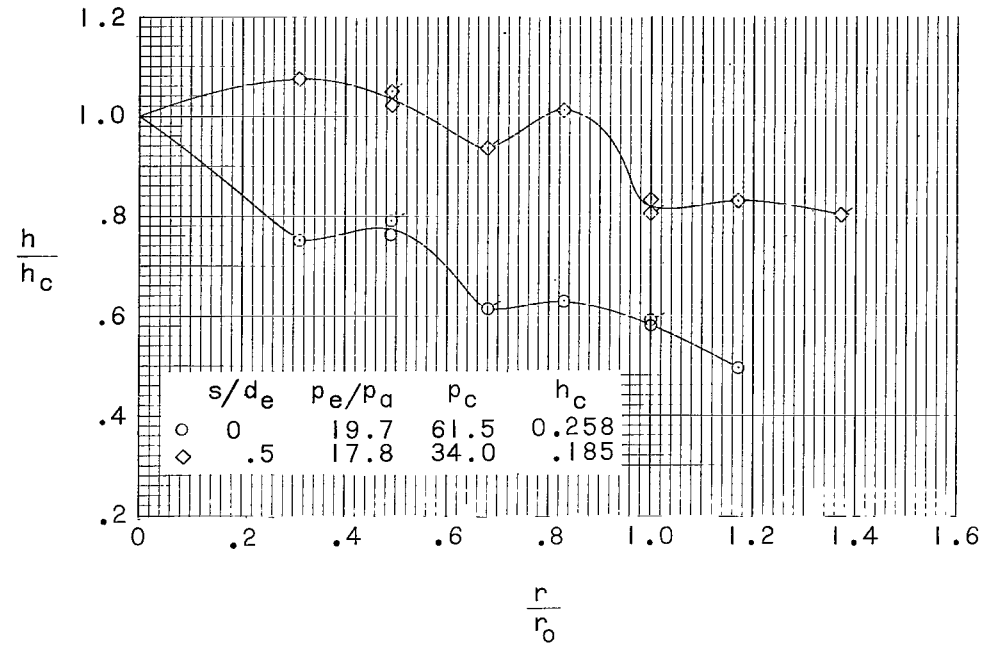


(a) Variable nozzle extension for $C_t/d_e = 0.35$. (Flagged data symbols represent data from first set of tests.)

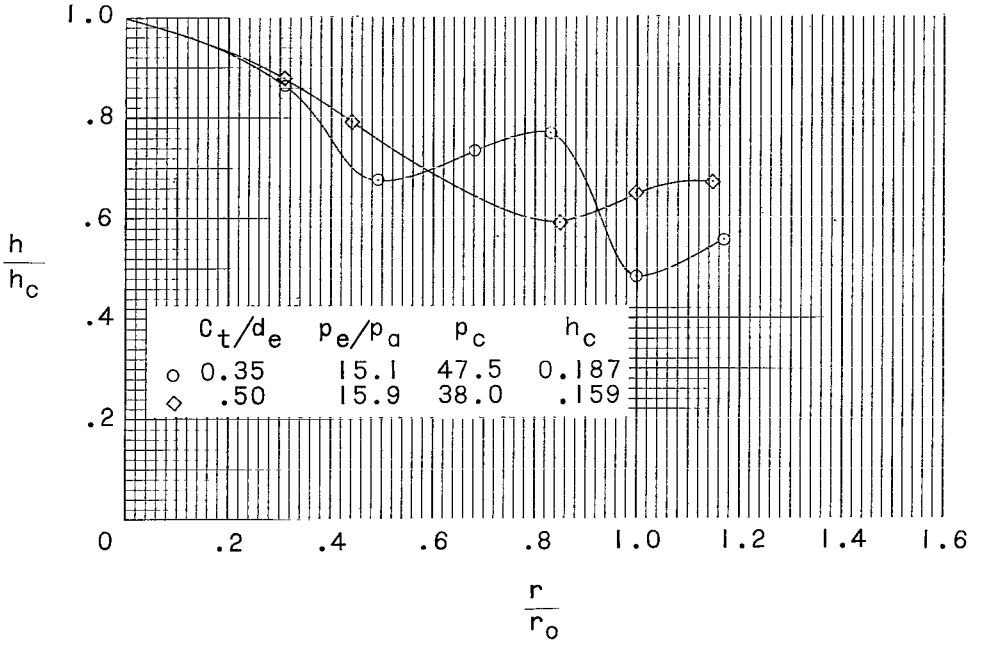


(b) Variable nozzle spacing for $s/d_e = 0$.

Figure 15.- Radial heat-transfer-coefficient distribution for choked backflow at N = 3.

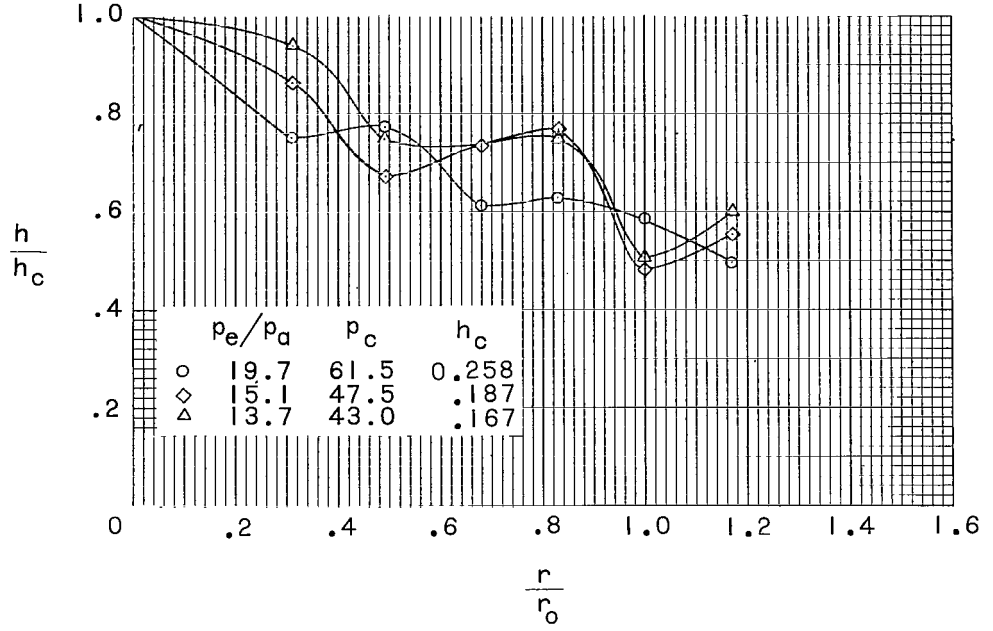


(c) Variable nozzle pressure ratio for $C_t/d_e = 0.35$ and $s/d_e = 0$.

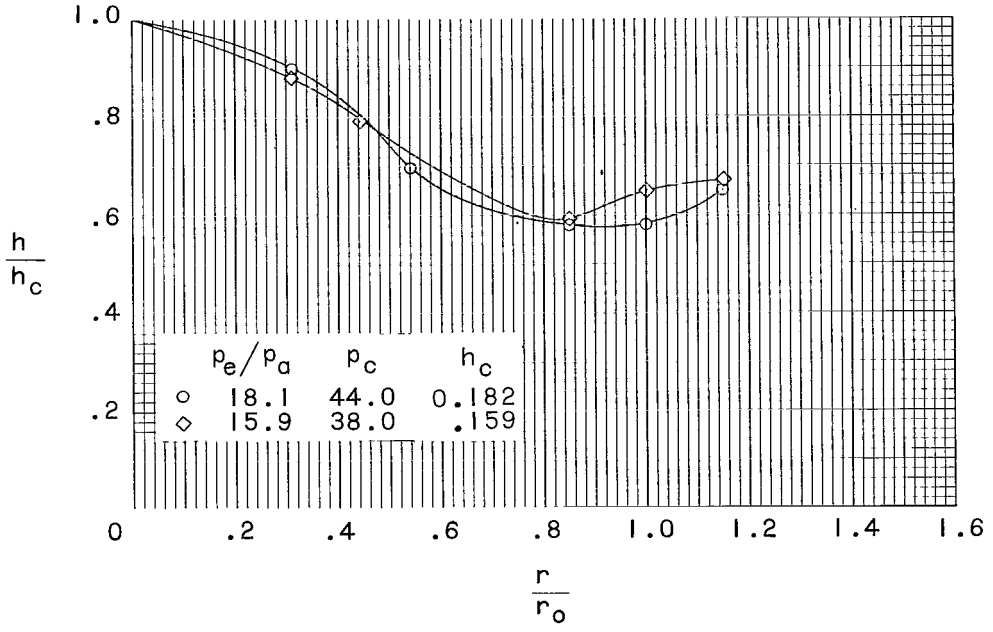


(d) Variable nozzle pressure ratio for $C_t/d_e = 0.50$ and $s/d_e = 0$.

Figure 15.- Concluded.

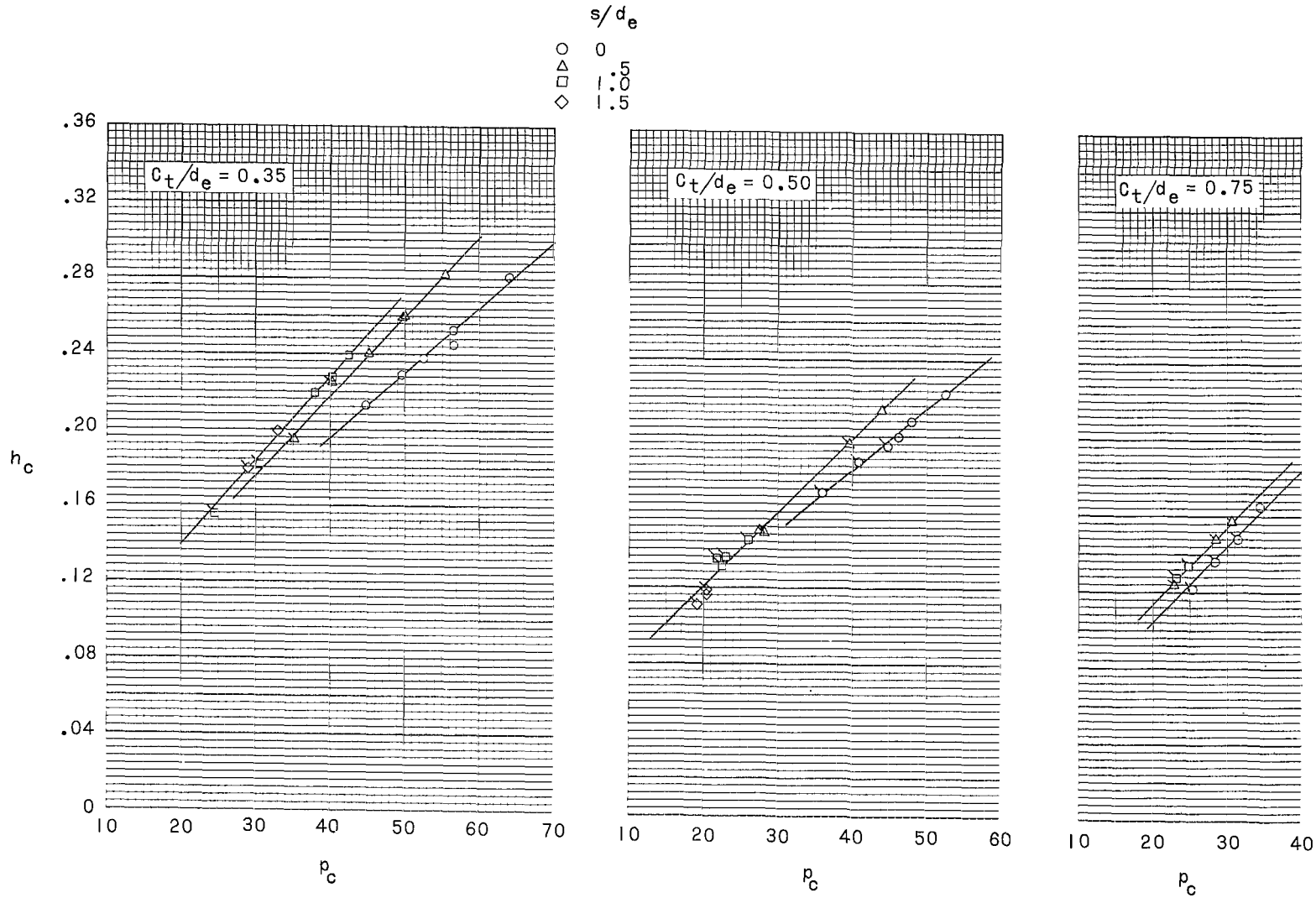


(a) N = 4.

Figure 16.- Variation of base-center heat-transfer coefficient with base-center pressure. (Flagged data symbols represent unchoked data.)

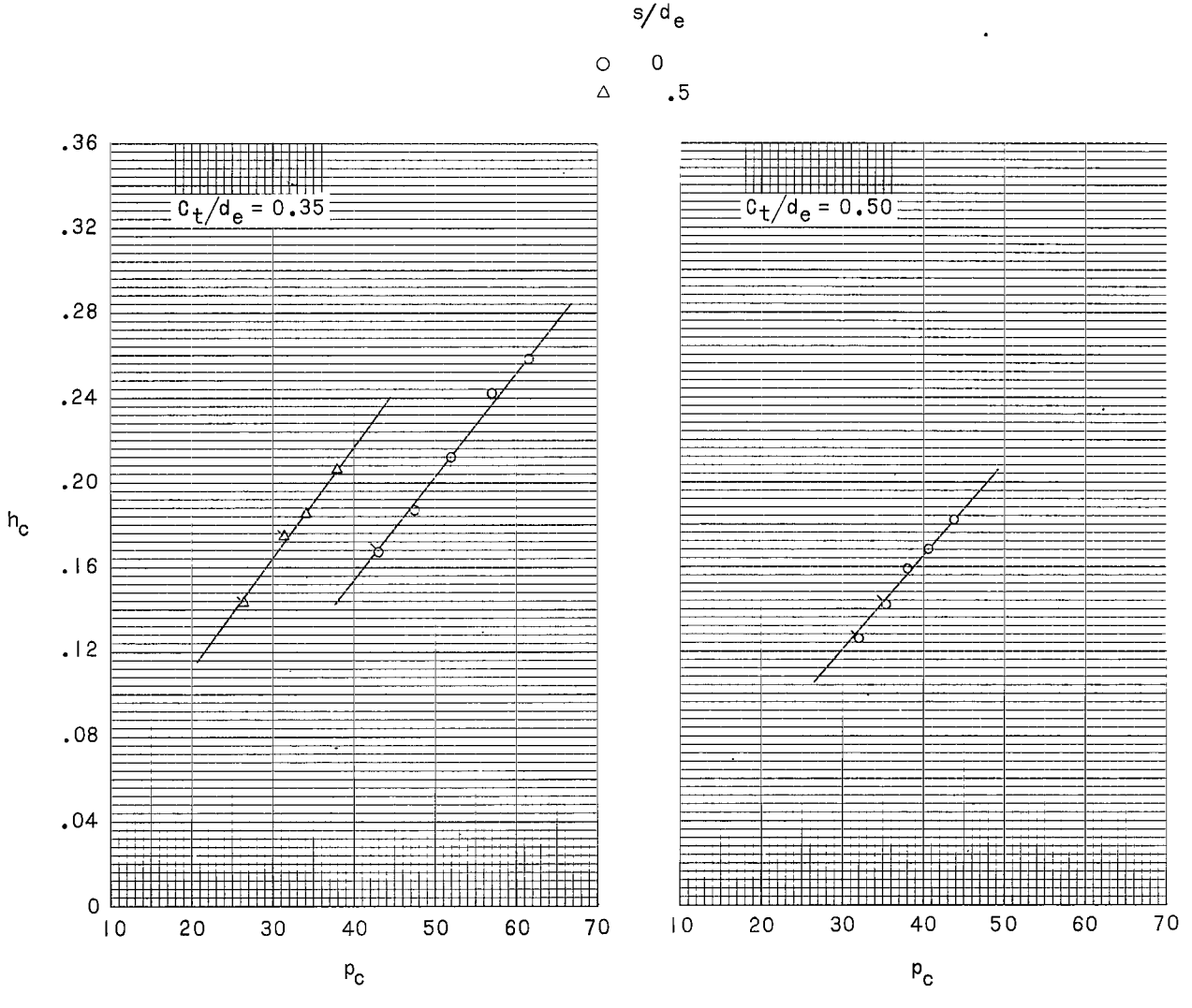


(b) N = 3.

Figure 16.- Concluded.

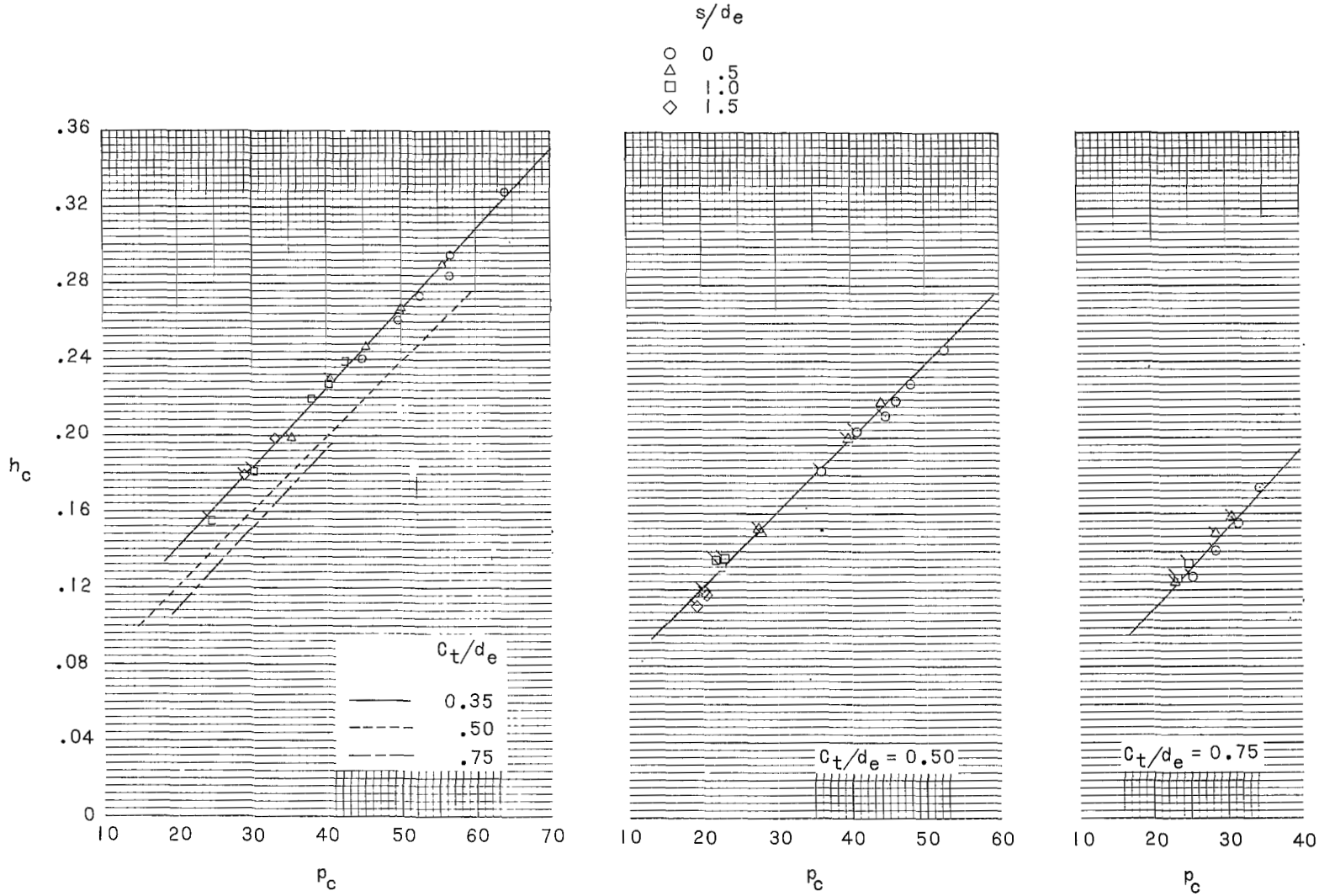


(a) N = 4.

Figure 17.- Variation of base-center heat-transfer coefficient with base-center pressure including a correction for base chilling. (Flagged data symbols represent unchoked data.)

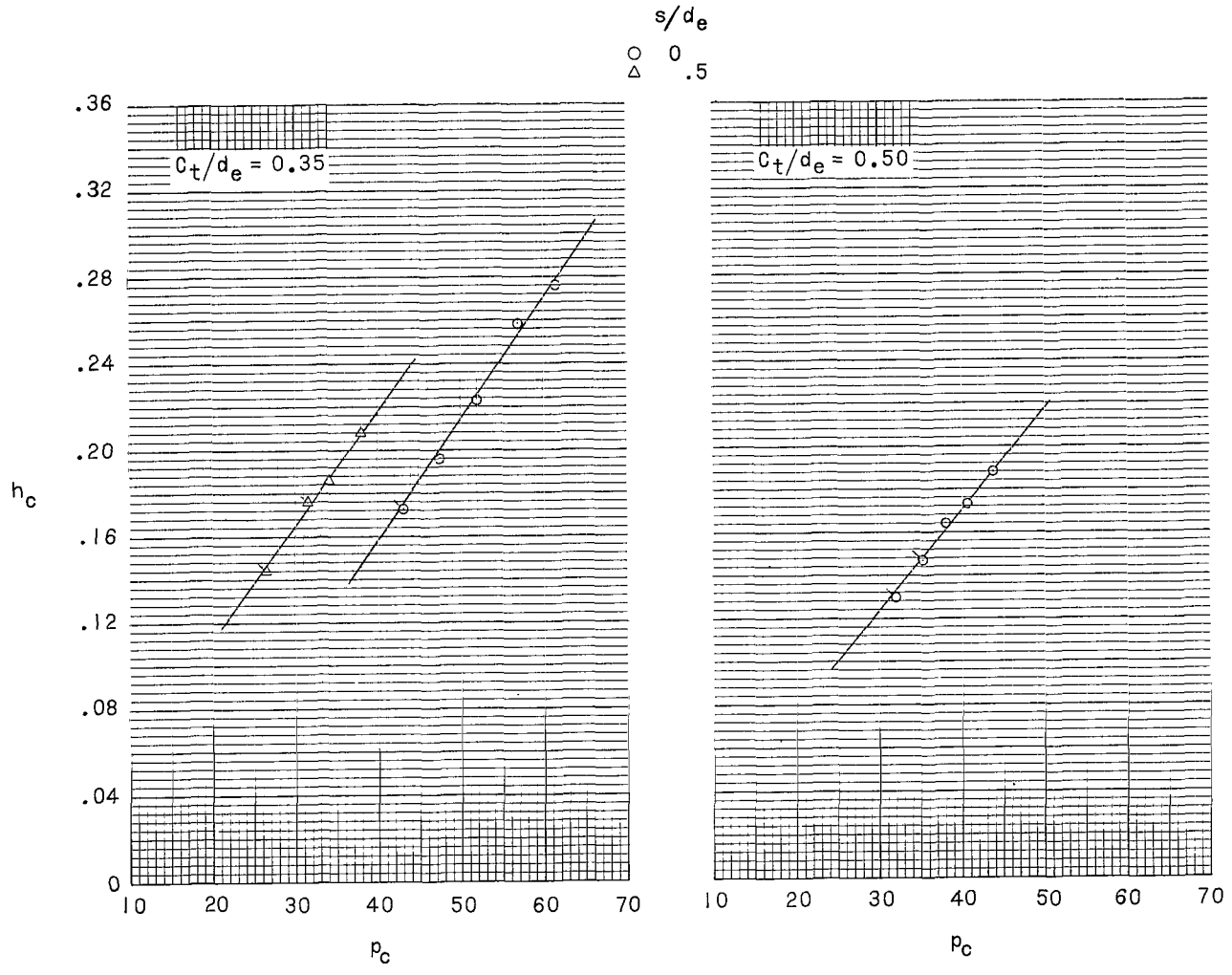


(b) N = 3.

Figure 17.- Concluded.

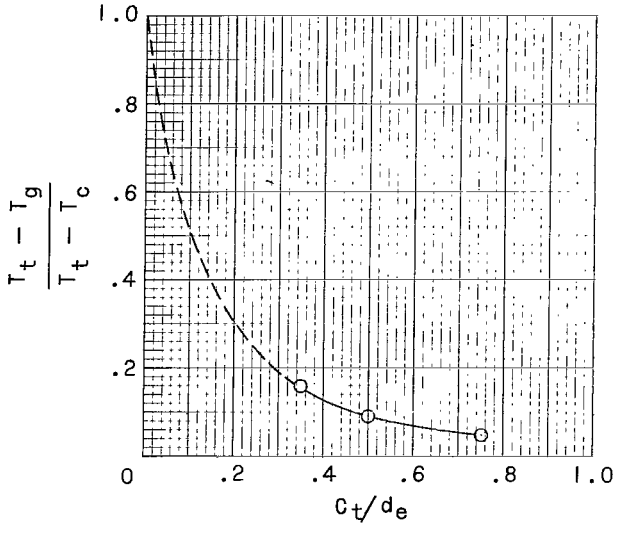


(a) Temperature ratio at constant $p_c$.

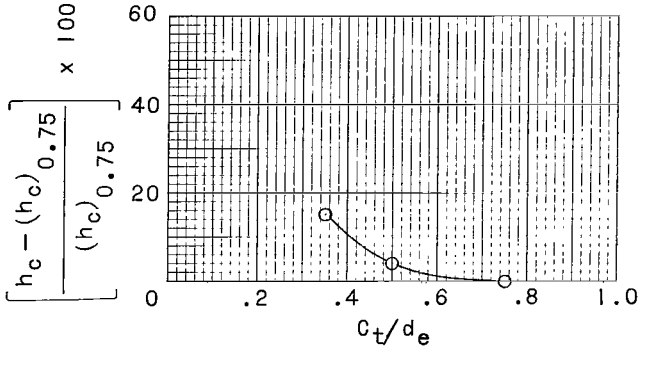


(b) Percent increase of $h_c$ at constant $p_c$.

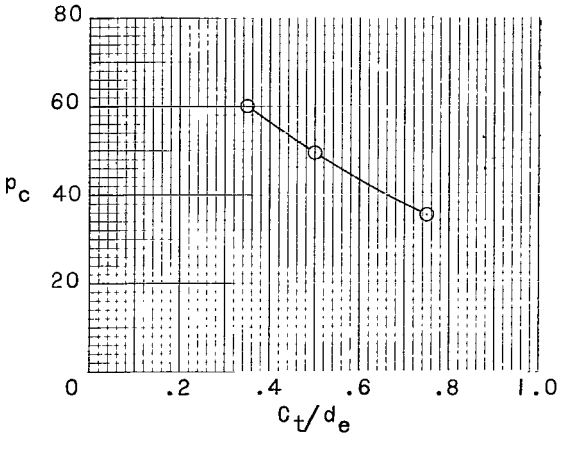


(c) Base-center pressure at $p_e/p_a = 18$.

Figure 18.- Variation of base-center properties with nozzle spacing for $s/d_e = 0$ and $N = 4$.

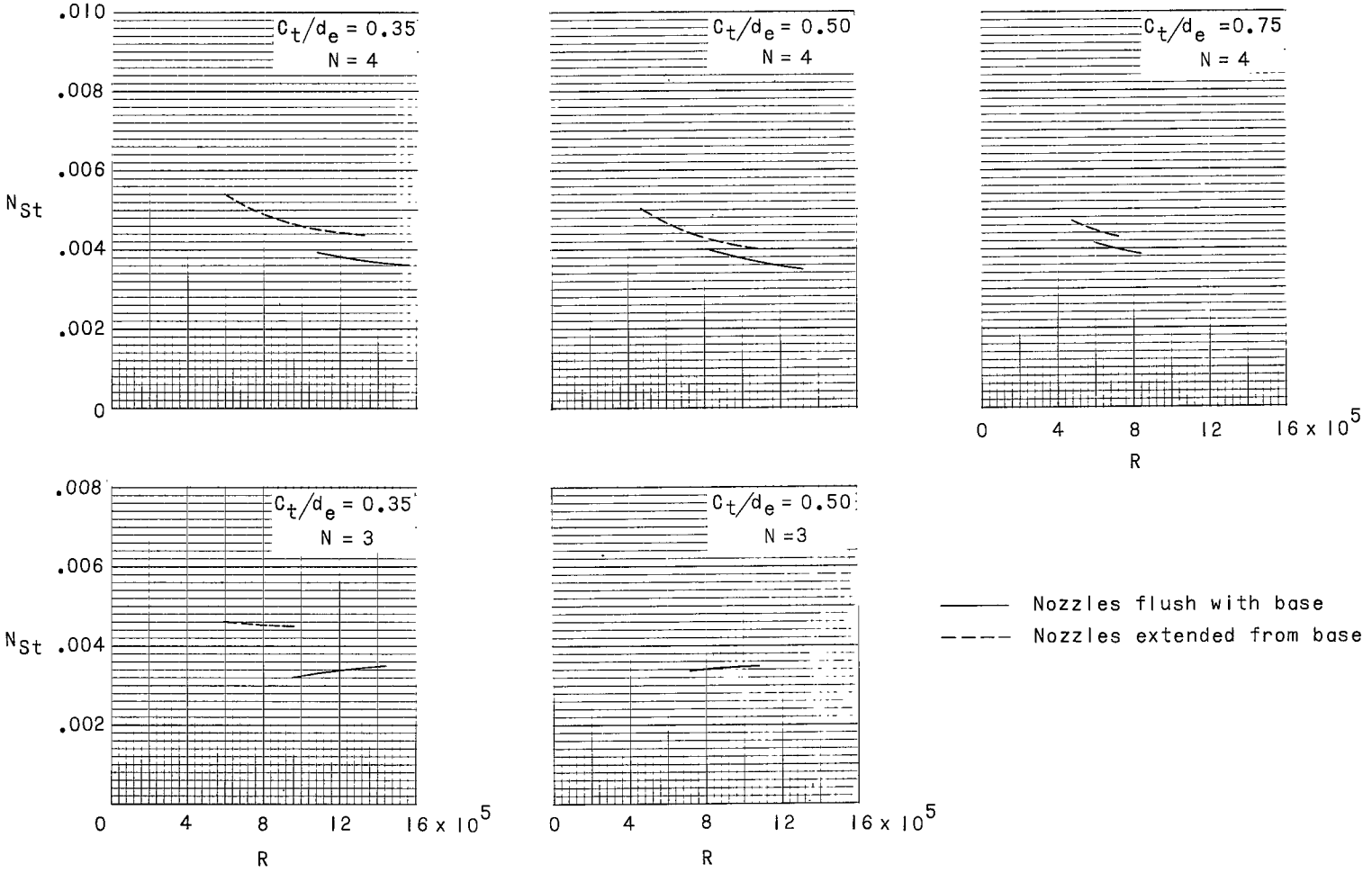


Figure 19.- Variation of Stanton number with Reynolds number at center of base.

-2172 (61)
00

*"The aeronautical and space activities of the United States shall be conducted so as to contribute . . . to the expansion of human knowledge of phenomena in the atmosphere and space. The Administration shall provide for the widest practicable and appropriate dissemination of information concerning its activities and the results thereof."*

—NATIONAL AERONAUTICS AND SPACE ACT OF 1958

# NASA SCIENTIFIC AND TECHNICAL PUBLICATIONS

TECHNICAL REPORTS: Scientific and technical information considered important, complete, and a lasting contribution to existing knowledge.

TECHNICAL NOTES: Information less broad in scope but nevertheless of importance as a contribution to existing knowledge.

TECHNICAL MEMORANDUMS: Information receiving limited distribution because of preliminary data, security classification, or other reasons.

CONTRACTOR REPORTS: Technical information generated in connection with a NASA contract or grant and released under NASA auspices.

TECHNICAL TRANSLATIONS: Information published in a foreign language considered to merit NASA distribution in English.

TECHNICAL REPRINTS: Information derived from NASA activities and initially published in the form of journal articles.

SPECIAL PUBLICATIONS: Information derived from or of value to NASA activities but not necessarily reporting the results of individual NASA-programmed scientific efforts. Publications include conference proceedings, monographs, data compilations, handbooks, sourcebooks, and special bibliographies.

***Details on the availability of these publications may be obtained from:***

**SCIENTIFIC AND TECHNICAL INFORMATION DIVISION**

**NATIONAL AERONAUTICS AND SPACE ADMINISTRATION**

**Washington, D.C. 20546**